Dalton Transactions

ROYAL SOCIETY OF CHEMISTRY

PAPER

View Article Online
View Journal | View Issue

Cite this: *Dalton Trans.*, 2023, **52**, 13689

Reactivity of Ir(I)-aminophosphane platforms towards oxidants†‡

Marco Palmese, Jesús J. Pérez-Torrente and Vincenzo Passarelli *

The iridium(I)-aminophosphane complex [Ir{κ^3*C,P,P'*-(SiNP-H)}(cod)] has been prepared by reaction of [IrCl(cod)(SiNP)] with KCH_3COO. DFT calculations show that this reaction takes place through an unexpected outer sphere mechanism (SiNP = $SiMe_2\{N(4\text{-}C_6H_4Me)PPh_2\}_2$; SiNP-H = $CH_2SiMe\{N(4\text{-}C_6H_4Me)PPh_2\}_2$). The reaction of [IrCl(cod)(SiNP)] or [Ir{κ^3*C,P,P'*-(SiNP-H)}(cod)] with diverse oxidants has been explored, yielding a range of iridium(III) derivatives. On one hand, [IrCl(cod)(SiNP)] reacts with allyl chloride rendering the octahedral iridium(III) derivative [$IrCl_2(\eta^3\text{-}C_3H_5)$(SiNP)], which, in turn, reacts with *tert*-butyl isocyanide yielding the substitution product [$IrCl(\eta^3\text{-}C_3H_5)(CN^tBu)$(SiNP)]Cl *via* the observed intermediate [$IrCl_2(\eta^1\text{-}C_3H_5)(CN^tBu)$(SiNP)]. On the other hand, the reaction of [Ir{κ^3*C,P,P'*-(SiNP-H)}(cod)] with $[FeCp_2]X$ (X = PF_6, CF_3SO_3), I_2 or $CF_3SO_3CH_3$ results in the metal-centered two-electron oxidation rendering a varied assortment of iridium(III) compounds. [Ir{κ^3*C,P,P'*-(SiNP-H)}(cod)] reacts with $[FeCp_2]^+$ (1 : 2) in acetonitrile affording [Ir{κ^3*C,P,P'*-(SiNP-H)}$(CH_3CN)_3$]$^{2+}$ isolated as both the triflato and the hexafluorophosphato derivatives. Also, the reaction of [Ir{κ^3*C,P,P'*-(SiNP-H)}(cod)] with I_2 (1 : 1) yields a mixture of iridium(III) derivatives, namely the mononuclear compound [IrI(κ^2*P,P'*-SiNP)(η^2,η^3-C_8H_{11})]I, containing the η^2,η^3-cycloocta-2,6-dien-1-yl ligand, and two isomers of the dinuclear derivative [Ir_2\{κ^3*C,P,P'*-(SiNP-H)\}$_2(\mu\text{-}I)_3$]I, the first species being isolated in low yield. DFT calculations indicate that [IrI(κ^2*P,P'*-SiNP)(η^2,η^3-C_8H_{11})]I forms as the result of a bielectronic oxidation of iridium(I) followed by the deprotonation of the cod ligand by iodide and the protonation of the methylene moiety of the [Ir{κ^3*C,P,P'*-(SiNP-H)}] platform by the newly formed HI. Finally, the oxidation of [Ir{κ^3*C,P,P'*-(SiNP-H)}(cod)] by methyl triflate proceeds *via* a hydride abstraction from the cod ligand, with the elimination of methane and the formation of the η^2,η^3-cycloocta-2,6-dien-1-yl ligand with the concomitant two-electron oxidation of the iridium centre. The crystal structures of selected compounds have been determined.

Received 24th July 2023,
Accepted 4th September 2023

DOI: 10.1039/d3dt02361c

rsc.li/dalton

Introduction

In the last decade, aminophosphanes have attracted increasing attention due to their modular synthesis[1] and their consequent suitability to tailor the steric and electronic properties of the resulting metal complex. Actually, a variety of mono and bidentate aminophosphano ligands have been reported, giving rise to a range of metal–ligand architectures[2–5] with applications including catalysis,[2] bond activation,[2a,3] redox-active multimetallic

Departamento de Química Inorgánica, Instituto de Síntesis Química y Catálisis Homogénea (ISQCH), Universidad de Zaragoza-CSIC, C/Pedro Cerbuna 12, ES-50009 Zaragoza, Spain. E-mail: passarel@unizar.es

† Dedicated to Prof. Guido Pampaloni, mentor and friend, on the occasion of his retirement, in recognition of his remarkable contributions to coordination and organometallic chemistry, and his extraordinary commitment to the education of generations of chemists.

‡ Electronic supplementary information (ESI) available: ^1H, $^{13}C\{^1H\}$-apt and $^{31}P\{^1H\}$ NMR spectra. Coordinates of calculated structures (*xyz*). CCDC 2282655–2282659. For ESI and crystallographic data in CIF or other electronic format see DOI: https://doi.org/10.1039/d3dt02361c

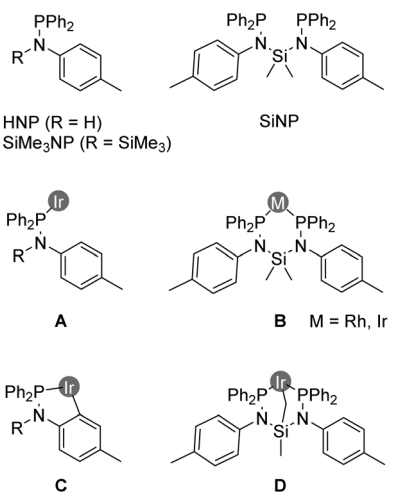

Fig. 1 Ligands RNP (R = H, $SiMe_3$) and SiNP and their coordination modes to rhodium[6] and iridium.[7]

systems[4] and metaloenzyme mimics.[5] On this background, our group has focussed on the preparation of rhodium[6] and iridium[7] derivatives with the aminophosphano ligands RNP (R = H, $SiMe_3$) and SiNP ($SiMe_2\{N(4\text{-tolyl})PPh_2\}_2$, Fig. 1) showing that besides the foreseeable coordination through phosphorus atom(s) of either monodentate RNP (A, Fig. 1) or bidentante SiNP ligands (B), intramolecular C–H oxidative addition processes give rise to unexpected κ^2C,P (C) and κ^3C,P,P' platforms (D).

Relevant to this paper, it is worth a mention that, so far, the κ^3C,P,P' coordination of SiNP has been found to be promoted by π-acceptor ligands like carbon monoxide,[7a] *tert*-butyl isocyanide[7d] and trimethyl phosphite,[7b] with the concomitant formation of an iridium(III)-hydride moiety (Scheme 1). Also, in our hands, the reactivity of the resulting iridium(III) complexes with substrates like alkynes or alkenes was observed to be absent plausibly due to the substitutional inertness of the ancillary ligands.[7a,b,d] Thus, we decided to explore alternative routes leading to the Ir{κ^3C,P,P'-(SiNP-H)} platform. More specifically, on one hand, we envisioned that the introduction of an allyl group at the Ir(κ^2P,P'-SiNP) moiety might trigger the deprotonation of one $SiCH_3$ group along with the elimination of propene, rendering the desired Ir{κ^3C,P,P'-(SiNP-H)} platform (SiNP-H = $CH_2SiMe\{N(4\text{-}C_6H_4Me)PPh_2\}_2$). On the other hand, we decided to explore the use of acetate as a Brønsted base in order to access the Ir{κ^3C,P,P'-(SiNP-H)} platform. Thus, we report herein the reaction of [IrCl(cod)(SiNP)] with either allyl chloride or potassium acetate and the study of the reactivity of the resulting metal complexes.

Results and discussion

Reaction of [IrCl(cod)(SiNP)] with allyl chloride

The iridium(I) complex [IrCl(cod)(SiNP)] reacts with allyl chloride affording almost quantitatively the iridium(III) derivative [$IrCl_2(\eta^3\text{-}C_3H_5)$(SiNP)] (**1**) as a result of the formal oxidative addition of the carbon–chlorine bond to iridium(I) and the release of the cod ligand (Scheme 2).

As shown in Fig. 2, the crystal structure of **1** reveals a distorted octahedral coordination polyhedron at the metal centre, similar to that already reported for [$RhCl_2(\eta^3\text{-}C_3H_5)$(SiNP)].[6] Indeed, the SiNP exhibits a κ^2P,P' coordination [P1–Ir–P2 92.08 (3)°] and the chlorido ligands adopt a mutually *cis* disposition

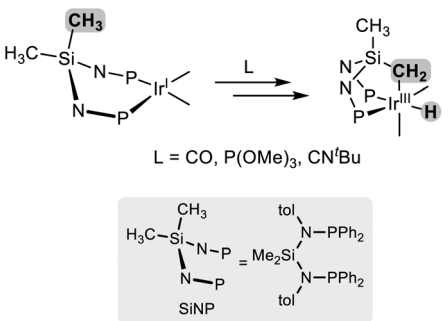

Scheme 1 Formation of the [Ir{κ^3C,P,P'-(SiNP-H)}] platform upon oxidative addition of the $SiCH_2$-H bond to iridium(I).[7a,b,d]

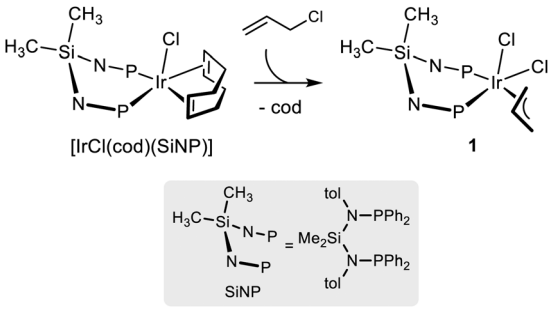

Scheme 2 Preparation of [$IrCl_2(\eta^3\text{-}C_3H_5)$(SiNP)] (**1**).

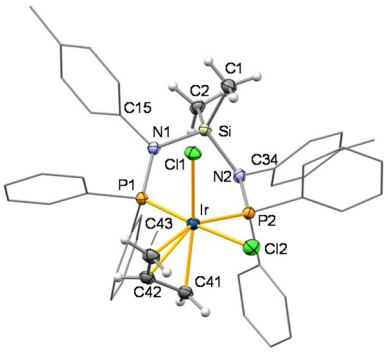

Fig. 2 ORTEP plot of **1**. For clarity, most hydrogen atoms are omitted, and tolyl and phenyl groups are shown in a wireframe style. Thermal ellipsoids are at 50% probability. Selected bond lengths (Å) and angles are (°): C41–Ir 2.138(4), C42–Ir 2.188(4), C43–Ir 2.277(4), P1–Ir 2.2676(9), P2–Ir 2.2959(9), Cl1–Ir 2.4469(9), Cl2–Ir 2.4566(9), C42–C41 1.440(5), C43–C42 1.388(6), N1–P1 1.681(3), N1–Si 1.758(3), N2–P2 1.697(3), N2–Si 1.765(3), C15–N1 1.455(4), C34–N2 1.461(4), P1–Ir–P2 92.08(3), Cl1–Ir–Cl2 88.10(3), P1–Ir–Cl2 176.63(3), C41–Ir–Cl1 160.35(10), C43–Ir–P2 160.13(11), N1–Si–N2 107.12(14), C1–Si–C2 108.27(18), C34–N2–P2 118.1(2), C15–N1–P1 120.6(2), C15–N1–Si 112.5(2), P1–N1–Si 126.94 (18), C34–N2–Si 110.7(2), P2–N2–Si 125.34(17).

[Cl1–Ir–Cl2 88.10(3)°] rendering a see–saw IrP_2Cl_2 fragments, with the η^3-allyl completing the coordination sphere of the metal. The resulting complex is chiral (Δ configuration is shown in Fig. 2), however it is worth noting that both enantiomers Δ and Λ are present in the crystal as a consequence of the centrosymmetric space group, namely, $P2_1/c$. Reasonably, as a consequence of the different *trans* influence of phosphorus (P2) and chlorine (Cl1), a non-symmetric coordination of the η^3-allyl ligand is observed. As a matter of fact, different metal–carbon bond lengths [Ir–C41 2.138(4), Ir–C42 2.188(4), Ir–C43 2.277(4) Å] are observed along with different carbon–carbon bonds [C41–C42 1.440(5), C42–C43 1.388(6) Å], similar to that observed in iridium-η^3-allyl systems reported in the literature.[8] Finally, as previously observed in related Ir-SiNP complexes,[7d,e] N1 and N2 exhibits an almost planar geometry ($\Sigma^\circ_{N1} = 360.0$, $\Sigma^\circ_{N2} = 354.1°$) with nitrogen–phosphorus (1.689 Å, av.), nitrogen–silicon (1.762 Å, av.) and nitrogen–carbon (1.438 Å, av.) bond lengths which suggest that nitrogen–phosphorus backdonation is operative to some extent and is responsible for the planar geometry of both N1 and N2.

As for the solution structure of **1**, at 298 K sharp well-shaped $^{31}P\{^1H\}$ doublets at 30.6 and 24.3 ppm ($^2J_{PP}$ = 25.2 Hz) are observed suggesting the presence of two non-equivalent phosphorus atoms occupying mutually *cis* coordination sites. On the other hand, broad ^1H signals between 6 and 8 ppm suggests that at room temperature the rotation of the tolyl and the phenyl groups around the N–C and P–C bonds, respectively, may be hindered. On this ground, the spectroscopic characterization of **1** was carried out at 233 K. At that temperature, two ^1H and two $^{13}C\{^1H\}$ resonances for the $SiCH_3$ groups are observed (δ_H, δ_C: 0.83, 2.4; −0.35, 2.7 ppm) confirming the presence of two different ligands at the axial positions (taking the IrP_2 plane as the equatorial plane). As for the η^3-allyl moiety, three ^{13}C resonances are observed at 102.9 (C^2), 72.1 (C^1) and 43.2 ppm (C^3) along with five ^1H signals (δ_H 4.84, C^2H; 4.03 and 3.94, C^1H_2; 2.06 and 1.43 ppm, C^3H_2).

Contrary to our expectation, compound **1** is thermally stable in toluene, neither elimination of propene nor decomposition being observed (^1H NMR) even after 18 h heating at reflux. In view of this thermal stability, the reaction of **1** with *tert*-butyl isocyanide was carried out in order to explore its reactivity. As a matter of fact, **1** reacts with *tert*-butyl isocyanide smoothly yielding [IrCl(η^3-C_3H_5)(CN^tBu)(κ^2*P,P*′-SiNP)]Cl (**2**Cl) as isocyanide ex/isocyanide exchange (Scheme 3).

The $^{31}P\{^1H\}$ NMR spectrum of **2**Cl contains two doublet at 28.3 and 25.9 ppm ($^2J_{PP}$ = 20.9 Hz) confirming the κ^2*P,P*′ coordination of SiNP. The ^1H and $^{13}C\{^1H\}$ NMR spectra are also indicative of the presence of the η^3-allyl moiety (δ_H 4.89, C^2H; 3.86, 3.72, C^1H; 2.31, 2.00 ppm, C^3H; δ_C 108.3, C^2; 63.6, C^1; 60.1 ppm, C^3) and of the *tert*-butyl isocyanide ligand (δ_H = 2.04, δ_C = 31.0 ppm). Interestingly, when the formation of **2**Cl was monitored by NMR spectroscopy, [$IrCl_2$(η^1-C_3H_5)(CN^tBu)(κ^2*P,P*′-SiNP)] (**3**) was observed as an intermediate (Scheme 3). In our hands, **3** could eventually be isolated along with around 20% of **1** (Fig. 3). Nonetheless, it was fully characterised in solution at 233 K, even in the presence of **1**. The $^{31}P\{^1H\}$ singlet at 31.9 ppm is indicative of two equivalent phosphorus atoms and, as a consequence, of a symmetric environment at the metal centre. Accordingly, two equivalent tolyl moieties are observed (δ_H 2.09, δ_C 20.9 ppm, CH_3^{tol}). Also, two ^1H signals at 0.47 (δ_C 4.5 ppm) and −0.05 ppm (δ_C 3.4 ppm) point at two non-equivalent $SiCH_3$ groups, confirming the presence of two different axial ligands (taking the IrP_2 plane as the equatorial plane). As for the allyl group, the ^1H and $^{13}C\{^1H\}$ NMR spectra show a pattern different from those observed for **1** and **2**Cl, which indicates an η^1 coordination. Indeed, two ^{13}C signals at 148.2 and 108.3 ppm are indicative of an uncoordinated olefinic $CH{=}CH_2$ group, whereas the signals at 3.34 (^1H) and 5.3 ppm (^{13}C) have been assigned to the $IrCH_2$ moiety. The *tert*-butyl isocyanide ligand (δ_H 1.06; δ_C 29.5 ppm, CH_3) completes the coordination sphere of the metal centre.

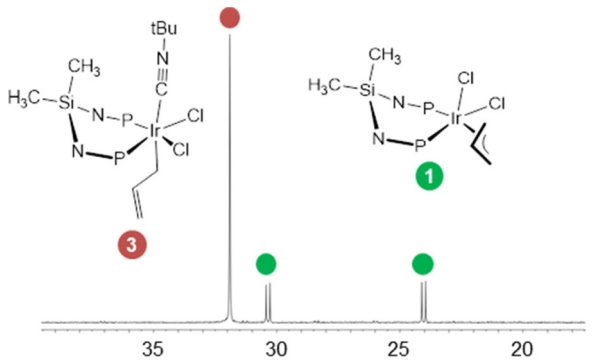

Fig. 3 $^{31}P\{^1H\}$ NMR spectrum of **3** in the presence 20 mol% of **1** (CD_2Cl_2, 233 K).

On this ground, the Cl^-/CN^tBu exchange reaction between **1** and *tert*-butyl isocyanide should follow an associative pathway taking advantage of the $\eta^3 \rightarrow \eta^1 \rightarrow \eta^3$ haptotropic shift of the allyl ligand (Scheme 4). In this regard, DFT calculations were performed in order to shed light on the reaction sequence leading to **2**Cl. Firstly, the $\eta^3 \rightarrow \eta^1$ shift of the allyl ligand in **1** renders the coordinatively unsaturated intermediate **I**. In turn, **I** isomerises to **II**, which ultimately reacts with *tert*-butyl isocyanide yielding the observed intermediate **3**. Afterwards, **3** should release one chlorido ligand (**3** → **III**Cl) and finally the $\eta^1 \rightarrow \eta^3$ shift should give rise to **2**Cl. As for the calculated relative Gibbs free energy of the proposed intermediates, the formation of both **3** and **2**Cl from **1** is calculated to be exergonic in agreement with the observed course of the reaction of **1** with *tert*-butyl isocyanide. As far as the calculated relative stability of **2**Cl *vs.* **3** is concerned, unaccounted solvation effects and/or underestimated ion pair stabilization for **2**Cl may be responsible for the calculated higher stability of **3** with respect to **2**Cl.

Depending on the topology of the $\eta^3 \rightarrow \eta^1$ shift in **1**, **IV** may also form (Scheme 4). Nonetheless, its formation is calculated to be significantly more endergonic than the formation of **I** and **II**, thus ruling out **IV** as a possible intermediate.

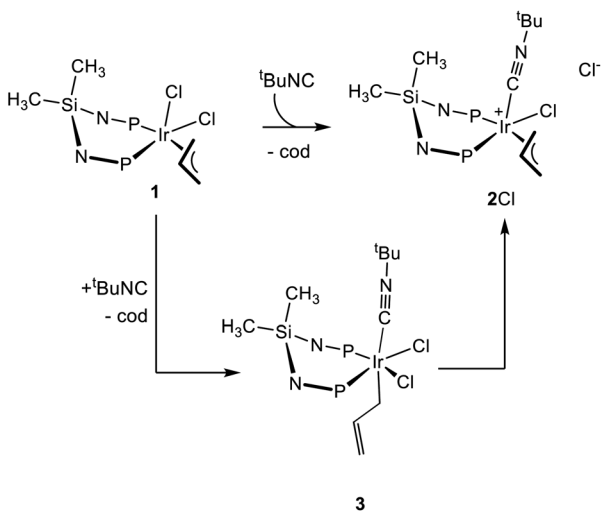

Scheme 3 Reaction of **1** with *tert*-butyl isocyanide.

Synthesis of [Ir{κ^3*C,P,P*′-(SiNP-H)}(cod)]

The reaction of [IrCl(cod)(SiNP)] with potassium acetate in dichloromethane smoothly affords the metallated iridium(I)

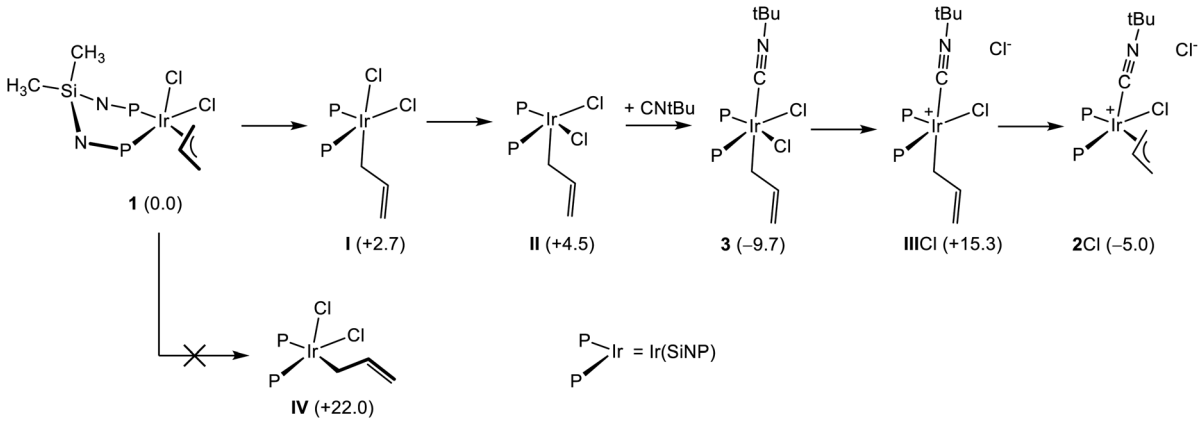

Scheme 4 Reaction sequence for the reaction of **1** with *tert*-butyl isocyanide along with the calculated values of relative Gibbs free energy (kcal mol^{-1}, B97D3/def2svp).

derivative [Ir{κ^3*C*,*P*,*P*′-(SiNP-H)}(cod)] (**4**) as a result of the deprotonation of one $SiCH_3$ moiety (Scheme 5). Remarkably, as mentioned before, previously reported Ir{κ^3*C*,*P*,*P*′-(SiNP-H)} platforms[7a,b,d] were obtained *via* $SiCH_2$-H oxidative addition to iridium(I) and, as a result, contained the iridium(III)-hydride moiety (Scheme 1), whereas in this case, for the first time, the reaction implies the base-assisted metal–carbon bond formation (*vide infra*), with no change of the metal oxidation state. The crystal structure of **4** reveals a distorted bipyramidal geometry at the metal centre (TBPY-5-23) with the ligand SiNP-H occupying three mutually *cis* positions [C1–Ir–P1 85.89(11)°, C1–Ir–P2 81.96(11)°, P1–Ir–P2 98.82(4)°] and the cod ligand completing the coordination sphere [CT1–Ir–CT2 84.910(15)°] (Fig. 4). Similar to what previously observed in the related iridium(I) complex [Ir{κ^3*C*,*P*,*P*′-(SiNP-H)}(CO)$_2$],[7a] the distance Ir–CT2 is longer than Ir–CT1 [Ir–CT1 2.0153(3), Ir–CT2 2.1007(3) Å] due to the high *trans* influence of the methylene group. Accordingly, the bond C41–C42 [1.447(6) Å] is longer than C45–C46 [1.409(6) Å] indicating a higher degree of backdonation to the coordinated olefinic bond lying in the equatorial plane. As for the κ^3*C*,*P*,*P*′-(SiNP-H) backbone, when compared with the uncomplexed SiNP ligand,[7d] the wider angle C1–Si–C2 [123.3(2)°] and the smaller angles P1–N1–Si [111.41(18)°] and P2–N2–Si [111.47(19)°] are reasonably the consequence of the metallation and the subsequent formation of two fused five-member cycles [SiNP: C1–Si–C2 111.48(10)°, P1–N1–Si 121.40(9)°, P2–N2–Si 120.94(9)°].[7d]

The solution structure of **4** is similar to that observed in the solid state. The $^{31}P\{^1H\}$ singlet at 47.1 ppm along with the

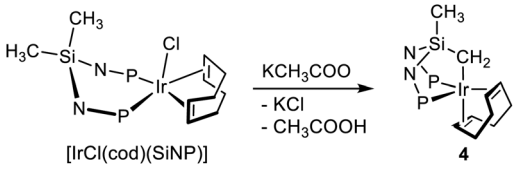

Scheme 5 Synthesis of [Ir{κ^3*C*,*P*,*P*′-(SiNP-H)}(cod)] (**4**).

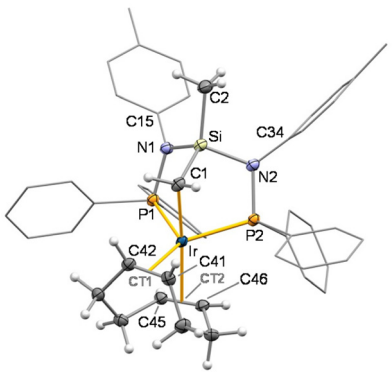

Fig. 4 ORTEP plot of **4**. For clarity, most hydrogen atoms are omitted, and tolyl and phenyl groups are shown in a wireframe style. Thermal ellipsoids are at 50% probability. Selected bond lengths (Å) and angles are (°): C1–Ir 2.167(4), P1–Ir 2.2976(10), P2–Ir 2.3451(10), Ir–CT1 2.0153(3), Ir–CT2 2.1007(3), C41–C42 1.447(6), C45–C46 1.409(6), N1–P1 1.701(3), N1–Si 1.759(3), N2–P2 1.704(3), N2–Si 1.770(4), C1–Ir–P1 85.89(11), C1–Ir–P2 81.96(11), P1–Ir–P2 98.82(4), CT1–Ir–CT2 84.910(15), CT1–Ir–C1 86.76(11), CT2–Ir–C1 171.59(11), CT1–Ir–P1 125.65(3), CT1–Ir–P2 133.11(3), C1–Si–C2 123.3(2), N1–Si–N2 113.45(16), C15–N1–P1 123.5(3), C15–N1–Si 124.4(3), P1–N1–Si 111.41(18), C34–N2–P2 124.5(3), C34–N2–Si 119.0(3), P2–N2–Si 111.47(19). CT1 and CT2 are the centroids of C41 and C42, and of C45 and C46, respectively.

$^1H/^1H\{^{31}P\}$ triplet/singlet at 0.14 ppm and the ^1H singlet at −0.83 ppm, assigned to the $SiCH_2Ir$ and $SiCH_3$ moieties, respectively, confirm that the κ^3*C*,*P*,*P*′ coordination is preserved in a symmetrical metal environment. Accordingly, two ^1H signals are observed at 3.60 and 2.60 ppm for the cod ligand. Notably, no cross peaks are observed between them in either the ^1H–^1H COSY or the ^1H–^1H NOESY spectra, thus ruling out the square pyramidal geometry SPY-5-32 for **4** in solution. Accordingly, the SPY-5-32 isomer was calculated to be less stable than **4** (TBPY-5-23) by 11.2 kcal mol^{-1} (*vide infra*).

The course of the formation of **4** was explored by means of DFT calculations (Fig. 5). Two mechanisms were considered,[9] one based on the well-established acetate-assisted C–H

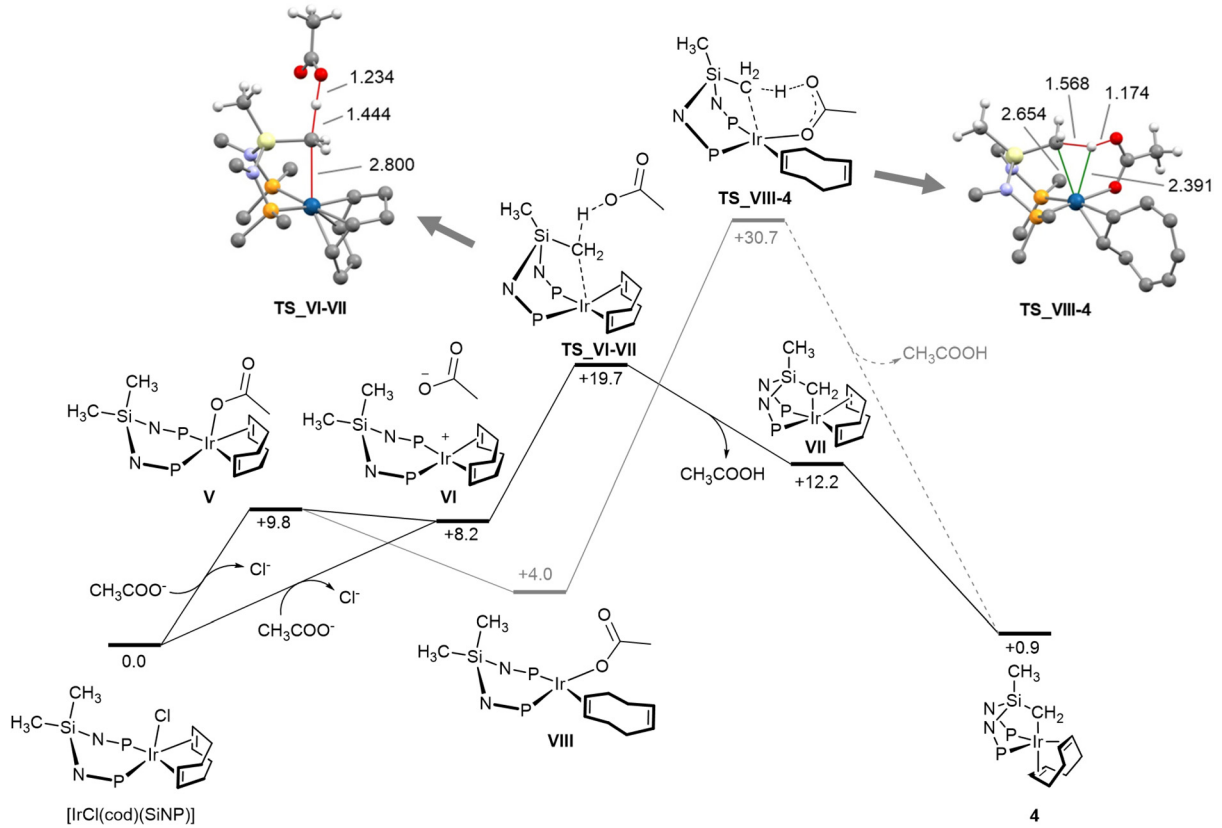

Fig. 5 Gibbs free energy profiles for the formation of [Ir{κ^3*C,P,P'*-(SiNP-H)}(cod)] (**4**) (black, outer sphere deprotonation; gray, acetate-assisted CH activation; kcal mol^{-1}, B97D3/def2svp), along with the calculated structures of **TS_VI-VII** and **TS_VIII-4** and selected interatomic distances (Å). Gray, carbon; white, hydrogen; violet, nitrogen; red, oxygen; yellow, silicon; orange, phosphorus, blue, iridium.

activation, and the other on the outer sphere deprotonation of the $SiCH_3$ moiety of [IrCl(cod)(SiNP)] by acetate. Fig. 5 shows the Gibbs free energy profiles for the two explored routes along with the structures of calculated transition states.

Considering the outer sphere mechanism, the first step should be the chloride abstraction/substitution to yield the pentacoordinate acetato derivative **V** or the square planar intermediate **VI**, or an equilibrium mixture of the two. In turn, **VI** should undergo metallation *via* an outer sphere interaction of the $SiCH_3$ moiety with free acetate ion. Indeed, acetate deprotonates the $SiCH_3$ group as long as the metal–carbon bond forms (**TS_VI-VII**). As a result, the square pyramidal derivative **VII** (SPY-5-32) forms which ultimately isomerises to the observed more stable trigonal bypiramidal product **4** (TBPY-5-23). The overall transformation [IrCl(cod)(SiNP)] + CH_3COO^- → **4** + CH_3COOH + Cl^- is calculated to be slightly endergonic (ΔG_r = +0.9 kcal mol^{-1}), thus the formation of solid potassium chloride should be decisive for the outcome of the reaction. Regarding the base-assisted C–H bond cleavage mechanism, starting from pentacoordinate acetato derivative **V**, the preliminary η^2, η^2 → η^2 haptotropic shift of the cod ligand should take place (**V** → **VIII**) in order to allow the required arrangement of the C–H bond, the metal centre and the acetato ligand. Once the square planar intermediate **VIII** forms, the acetate assisted deprotonation/metalation of the $SiCH_3$ moiety takes place *via* the transition state **TS_VIII-4**. A thorough examination of interatomic distances in **TS_VIII-4** (Fig. 5) indicates that no metal–hydrogen interaction should exist thus ruling out any oxidative character of the $SiCH_2$-H bond cleavage.[9] From an energy standpoint, the acetate-assisted C–H activation mechanism is not a competitive route and should be ruled out, since the **TS_VIII-4** (+30.7 kcal mol^{-1}) is not accessible under the experimental conditions. On the other hand, the calculated activation barrier (**TS_VI-VII**, +19.7 kcal mol^{-1}) for the outer sphere mechanism nicely fits in with the observed outcome under the experimental conditions.

The endergonic character of the formation of **4** prompted us to carry out the reaction of **4** with triflic acid, as a strong Brønsted acid, in order to establish if the metalation of SiNP could be reverted, *i.e.* the Ir-CH_2Si could be protonated. As a matter of fact, when CF_3SO_3H was added to a CD_2Cl_2 solution of **4** (1 : 1 molar ratio) in an NMR tube, the instantaneous complete conversion of **4** to [Ir(cod)(SiNP)]$^+$ was observed, as established by comparison with the $^{31}P\{^1H\}$ and ^1H NMR data previously reported for [Ir(cod)(SiNP)]$^+$.[7a] Accordingly, on top of that, the reaction **4** + CF_3SO_3H → [Ir(cod)(SiNP)]$^+$ + $CF_3SO_3^-$ was calculated to be highly exergonic (−22.7 kcal mol^{-1}) likely as a consequence of the strong acidic character of CF_3SO_3H. In

this respect, it is worth mentioning that in a previous study[7d] the reactivity of the iridium(III) derivative [IrH{κ³*C*,*P*,*P*′-(SiNP-H)}(CN^{t}Bu)$_2$][PF$_6$] towards Brønsted acids, such as HBF$_4$, HPF$_6$ and CF$_3$COOH, was explored, showing that the Ir-CH$_2$Si bond is not reactive, rather the Si–N bonds break as a result of the formal addition of HF (formed *in situ* by reaction of PF_6^- with either CF$_3$COOH or HBF$_4$). On these grounds, the stability of the Ir{κ³*C*,*P*,*P*′-(SiNP-H)} platform towards Brønsted acids seems to be subtly determined by the oxidation state of the metal centre, the metal–carbon bond being reactive towards H^+ only in the case of iridium(I).

Reaction of [Ir{κ³*C*,*P*,*P*′-(SiNP-H)}(cod)] with oxidants

In order to expand the family of iridium complexes with the κ³*C*,*P*,*P*′-(SiNP-H) ligand, the reactivity of **4** towards oxidants, namely [FeCp$_2$]X (X = PF$_6$, CF$_3$SO$_3$), I$_2$ or CF$_3$SO$_3$Me, was explored.

4 undergoes a two-electron oxidation when treated with $[FeCp_2]^+$ (Ir : Fe 1 : 2 molar ratio) in acetonitrile affording the octahedral cation $[Ir\{\kappa^3C,P,P'\text{-(SiNP-H)}\}(CH_3CN)_3]^{2+}$ (**5**$^{2+}$) isolated as either the trifluromethanesulfonate or the hexafluorophosphate salt (Scheme 6).

Crystal structure of **5**[CF$_3$SO$_3$]$_2$ shows an octahedral coordination polyhedron at the metal centre with a facial coordination of the κ³*C*,*P*,*P*′-(SiNP-H) ligand [C1–Ir–P1 85.81(9)°, C1–Ir–P2 83.12(8)°, P1–Ir–P2 96.27(3) Å] (Fig. 6). The three remaining coordination sites are occupied by acetonitrile ligands. Noticeably, as a consequence of the higher *trans* influence of the metallated SiCH$_2$ moiety, the iridium–nitrogen N42–Ir [2.117(3) Å] is longer than N45–Ir [2.071(3) Å] and N48–Ir [2.091(3) Å]. When comparing the κ³*C*,*P*,*P*′-(SiNP-H) ligand in **5**$^{2+}$ and **4**, regardless of the oxidation state of the metal centre, the IrCH$_2$SiCH$_3$(NP)$_2$ backbones are virtually superimposable, minor differences being observed exclusively in the orientation of the phenyl and tolyl groups, probably as a consequence of the steric hindrance of ancillary ligands and/or the coordination polyhedron. The NMR spectra of **5**$^{2+}$ confirm that the solid state structure is preserved in solution. Actually, two sets of signals are observed in both the ^{1}H and the ^{13}C{^{1}H} NMR spectra for the acetonitrile ligand, namely at δ_H 2.24 ppm and δ_C 3.2 ppm for the acetonitrile ligands *trans* to phosphorus and at δ_H 2.44 and δ_C 3.9 ppm for the acetonitrile ligand *trans* to carbon. As for the SiNP-H ligand, in agreement with the proposed structure, one ^{31}P{^{1}H} NMR signal at 18.2 ppm indicates the equivalence of the two phosphorus atoms. Also, the ^{1}H and ^{13}C{^{1}H} signals at 1.46 and at −19.6 ppm, respectively, are assigned to the metallated methylene group, whereas the ^{1}H and ^{13}C{^{1}H} signals at 0.36 and −1.3 ppm, respectively, are assigned to the SiCH$_3$ group.

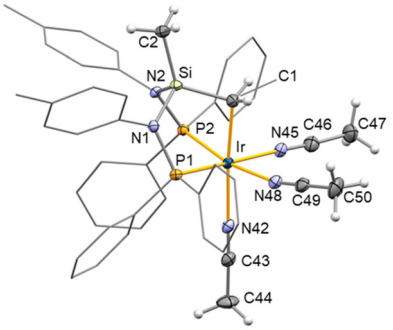

Fig. 6 ORTEP plot of **5**$^{2+}$ in **5**[CF$_3$SO$_3$]$_2$. For clarity, most hydrogen atoms are omitted, and tolyl and phenyl groups are shown in a wire-frame style. Thermal ellipsoids are at 50% probability. Selected bond lengths (Å) and angles are (°): N42–Ir 2.117(3), N45–Ir 2.071(3), N48–Ir 2.091(3), P1–Ir 2.2994(8), P2–Ir 2.3012(8), C1–Ir 2.105(3), N1–P1 1.687(2), N1–Si 1.757(3), N2–P2 1.678(2), N2–Si 1.780(2), C1–Ir–P1 85.81(9), C1–Ir–P2 83.12(8), P1–Ir–P2 96.27(3), C1–Ir–N42 175.88(10), N45–Ir–P1 171.92(7), N48–Ir–P2 168.94(7).

The treatment of **4** with I$_2$ (1 : 1) affords a mixture of three products, namely the iridium(III) derivatives [IrI(κ²*P*,*P*′-SiNP)(η²,η³-C$_8$H$_{11}$)]I (**6I**) and two isomers of the dinuclear species [Ir$_2${κ³*C*,*P*,*P*′-(SiNP-H)}$_2$(μ-I)$_3$]I (**7aI** and **7bI**), in a molar ratio **6**$^+$: **7a**$^+$: **7b**$^+$ 54 : 33 : 13 (Scheme 7, top). The mixture of **7a**PF$_6$ and **7b**PF$_6$ was independently prepared either by reaction of **4** with [FeCp$_2$][PF$_6$] in acetone and subsequent addition of NaI, or by direct reaction of **5**[PF$_6$]$_2$ with NaI (Ir : I = 2 : 3) (Scheme 7 and Fig. 7). On the other hand, **6I** was isolated in low yields from the mixture **6I** + **7aI** + **7bI** upon recrystallization from CH$_3$CN/Et$_2$O (Fig. 7).

The crystal structure of **6I** shows a virtually octahedral geometry at the metal centre with a bidentate κ²*P*,*P*′ coordination of SiNP [P1–Ir 2.3215(13) Å, P2–Ir 2.3442(13) Å, P1–Ir–P2 91.53(4)°] (Fig. 8). The iodido ligand lies *cis* to both phosphorus atoms [I1–Ir 2.7247(4) Å, P1–Ir–I1 90.94(3)°, P2–Ir–I1 93.04(3)°] with the cycloocta-2,6-dien-1-yl ligand formally occupying the three remaining coordination sites. Notably, the olefinic moiety lies *trans* to one phosphorus atom [Ir–CT 2.2494(2) Å, CT–Ir–P1 171.79(3)°], and the allyl moiety spans the remaining coordination sites *trans* to P2 and I1 [C43–Ir 2.294(5) Å, C42–Ir 2.200(5) Å, C41–Ir 2.278(6) Å, C41–Ir–I1 155.72(14)°, C43–Ir–P2 169.58(15)°]. To the best of our knowledge, only few examples of cod activation leading to the formation of the cycloocta-2,6-dien-1-yl ligand have been reported for iridium complexes.[10] NMR spectra indicate that the solution structure of **6**$^+$ is similar to that observed in the solid state. As a matter of fact, two ^{31}P{^{1}H} NMR doublets (δ_P 32.1, 23.2 ppm, $^2J_{PP}$ = 25.3 Hz) are observed for the two non-equivalent phosphorus atoms. In addition, the ^{1}H and ^{13}C{^{1}H} NMR signals assigned to the C$_8$H$_{11}$ ligand (Scheme 7, bottom) confirm the presence of the cycloocta-2,6-dien-1-yl ligand.

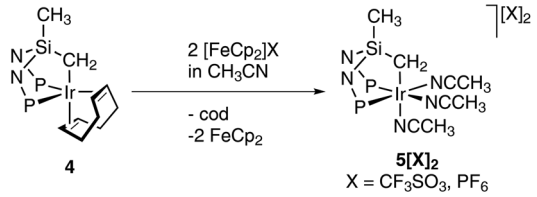

Scheme 6 Synthesis of [Ir{κ³*C*,*P*,*P*′-(SiNP-H)}(CH$_3$CN)$_3$][X]$_2$ (**5**[X]$_2$).

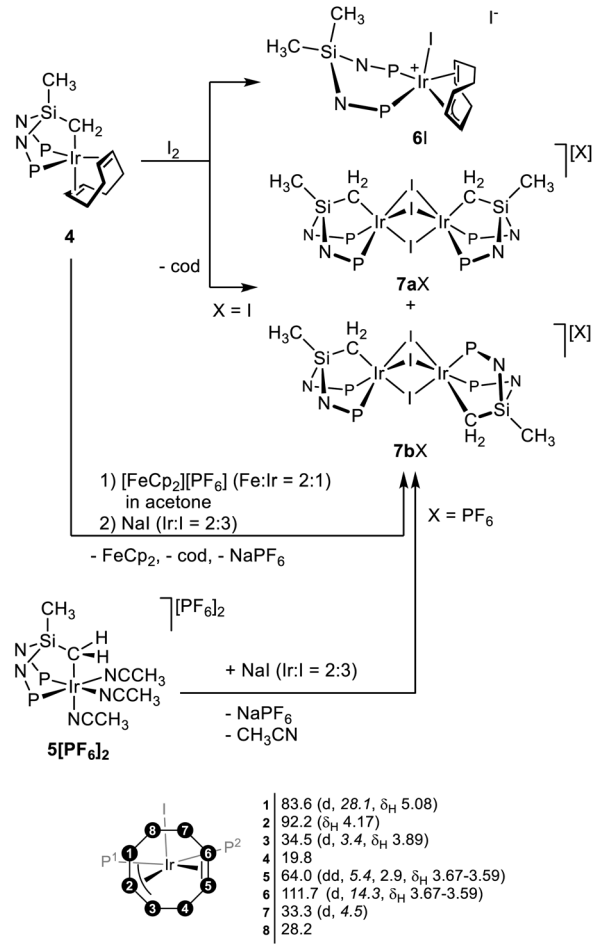

Scheme 7 (Top) Synthesis of **6**I, **7a**X and **7b**X (X = I, PF_6). (Bottom) Selected NMR data for $\mathbf{6}^+$ [δ_C, along with J_{CP}, italics, and δ_H (CD_2Cl_2)].

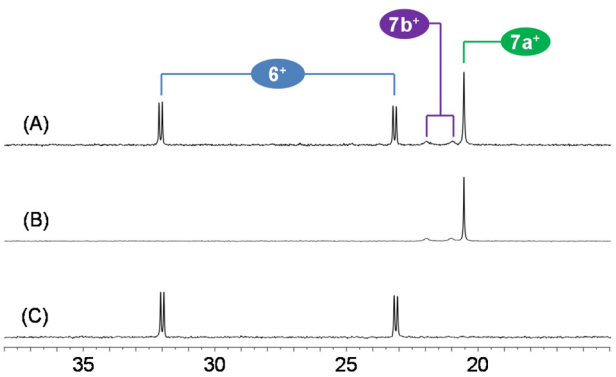

Fig. 7 $^{31}P\{^1H\}$ NMR spectra (CD_2Cl_2, 298 K) of (A) the solid mixture resulting from the reaction of **4** with I_2; (B) $\mathbf{7a}^+$ + $\mathbf{7b}^+$ obtained from the reaction of **5**$[PF_6]_2$ with NaI; (C) **6**I after recrystallization of a mixture of **6**I + **7a**I + **7b**I from CH_3CN/Et_2O.

Regardless of the synthetic route, a mixture of $\mathbf{7a}^+$ and $\mathbf{7b}^+$ (70 : 30, aprox.) was always obtained and, in our hands, it could not be separated. In addition, heating a solution containing a mixture of $\mathbf{7a}^+$ and $\mathbf{7b}^+$ resulted in the coalescence of

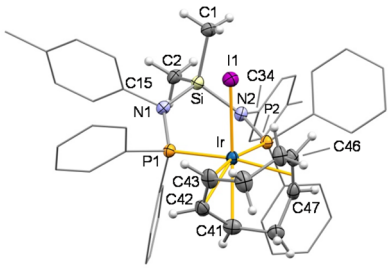

Fig. 8 ORTEP plot of $\mathbf{6}^+$ in **6**I. For clarity, most hydrogen atoms are omitted, and tolyl and phenyl groups are shown in a wireframe style. Thermal ellipsoids are at 50% probability. Selected bond lengths (Å) and angles are (°): P1–Ir 2.3215(13), P2–Ir 2.3442(13), I1–Ir 2.7247(4), C41–Ir 2.278(6), C42–Ir 2.200(5), C43–Ir 2.294(5), Ir–CT 2.2494(2), C41–C42 1.422(8), C42–C43 1.404(8), C46–C47 1.377(8), C41–Ir–I1 155.72(14), C42–Ir–I1 123.76(16), C43–Ir–I1 90.23(16), P1–Ir–P2 91.53(4), P1–Ir–I1 90.94(3), P2–Ir–I1 93.04(3), CT–Ir–I1 97.262(10), CT–Ir–P1 171.79(3), CT–Ir–P2 88.27(3), C41–Ir–P2 108.65(14), C42–Ir–P2 142.90(17), C43–Ir–P2 169.58(15), C15–N1–P1 118.2(3), C15–N1–Si 112.2(3), P1–N1–Si 129.3(3), C34–N2–P2 116.5(3), C34–N2–Si 111.6(3), P2–N2–Si 131.6(3). CT, centroid of C46 and C47.

their ^{31}P signals, suggesting that an equilibrium between the two isomers could be operative in solution. Finally, the MALDI-TOF mass spectra uniquely revealed one molecular peak at m/z 2040.8 (calcd. 2041.1, $[M]^+$) which suggests that $\mathbf{7a}^+$ and $\mathbf{7b}^+$ might be isomers. The crystal structure of $\mathbf{7a}^+$ (in **7a**PF_6) shows a dinuclear [Ir(μ-I)$_3$Ir] core [see Fig. 9 for Ir–I bond lengths and Ia–Ir–Ib angles] featuring a non-interaction intermetallic distance [Ir1···Ir2 3.7116(16) Å], with one κ^3C,P,P'-(SiNP-H) ligand completing the coordination sphere of each metal centre. The methylene moieties lie *trans* to the same iodido ligand (I2) rendering a virtual C_{2v} symmetry with two equivalent phosphorus atoms. As a consequence of the higher *trans* influence of the $SiCH_2$ group when compared to the PPh_2N moiety, the Ir1–I2 [2.7909(9) Å] and Ir2–I2 [2.8105(9) Å]

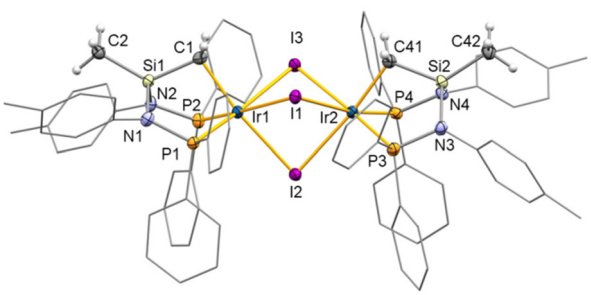

Fig. 9 ORTEP plot of $\mathbf{7a}^+$ in **7a**PF_6. For clarity, most hydrogen atoms are omitted, and tolyl and phenyl groups are shown in a wireframe style. Thermal ellipsoids are at 50% probability. Selected bond lengths (Å) and angles are (°): I1–Ir1 2.7308(8), I1–Ir2 2.7342(8), I2–Ir1 2.7909(9), I2–Ir2 2.8105(9), I3–Ir2 2.7316(8), I3–Ir1 2.7386(9), P1–Ir1 2.3037(15), P2–Ir1 2.2902(15), P3–Ir2 2.2886(15), P4–Ir2 2.3096(15), C1–Ir1 2.132(5), C41–Ir2 2.149(5), C1–Ir1–P2 83.36(13), C1–Ir1–P1 84.84(14), P2–Ir1–P1 97.36(6), C41–Ir2–P3 84.65(13), C41–Ir2–P4 84.44(14), P3–Ir2–P4 98.25(6), I1–Ir1–I3 77.36(3), I1–Ir1–I2 80.95(3), I3–Ir1–I2 80.80(3), I3–Ir2–I1 77.42(3), I3–Ir2–I2 80.57(3), I1–Ir2–I2 80.54(3).

bond lengths are longer than the remaining iridium–iodine bond lengths [Ir1–I1 2.7308(8), Ir1–I3 2.7386(9), Ir2–I1 2.7342(8), Ir2–I3 2.7316(8) Å]. The NMR spectra of **7a**$^+$ suggest that its structure in solution is similar to that in the solid state. Actually, one $^{31}P\{^1H\}$ singlet was observed at 20.7 ppm along with one ^1H and one $^{13}C\{^1H\}$ signal for the methyl group of the tolyl fragment [δ_H 2.05; δ_C 21.5 ppm] confirming the equivalence of the two SiNP arms. On the other hand, the resonances at δ_H 2.05 and 0.00 ppm as well as at δ_C −11.7 and −0.6 ppm are assigned to the $IrCH_2Si$ and $SiCH_3$ moieties, respectively.

As for **7b**$^+$, full characterization could not be achieved. Nonetheless, in view of the two resonances at δ_P 22.0 and 21.0 ppm ($\Delta\nu_{1/2}$ = 50 Hz), the $SiCH_2$ moieties are proposed to lie *trans* to different bridging iodine atoms at the [Ir(μ-I)$_3$Ir] core, thus rendering a virtual C_2 symmetry with two non-equivalent phosphorus atoms slowly exchanging on the NMR timescale at 298 K. As a confirmation, the relative Gibbs free energy for **7a**$^+$ (0.0) and **7b**$^+$ (+1.3 kcal mol^{-1}) nicely confirms that **7b**$^+$ should be observed in solution along with **7a**$^+$ (*vide infra*).

The course of the reaction of **4** with I_2 has been investigated by DFT calculations (Scheme 8). As a result of the two-electron oxidation of **4**, the iridium(III) species **IX**$^{2+}$ is assumed to be the starting point of two independent pathways, leading to either **6**$^+$ or **7a/b**$^+$, respectively. As for the formation of **7a/b**$^+$, the cod ligand of **IX**$^+$ should be displaced by incoming iodide rendering the dinuclear species **7a**$^+$ or **7b**$^+$. On the other hand, when dealing with the formation of **6**$^+$, the iodido ligand should dissociate (**IX**$^+$ → **X**$^{2+}$**I**$^-$) and eventually act as a base, abstracting H^+ from the cod ligand of **X**$^{2+}$ (**X**$^{2+}$**I**$^-$ → **XI**$^+$ + HI). Thereafter, the intermediate **XI**$^+$, that contains the η^2,η^3-cycloocta-2,6-dien-1-yl ligand, should react with the newly formed HI undergoing the protonation of the methylene group $IrCH_2Si$, finally yielding **6**$^+$ (the structures of the transition state **TS_X^{2+}I$^-$-XI$^+$** and **TS_XI$^+$-6$^+$** are shown in Scheme 8). For the sake of comparison, the isomer **XII**$^+$ of [IrI(κ^2*P*,*P*′-SiNP)(η^2,η^3-C_8H_{11})]$^+$ was calculated to be 9.1 kcal mol^{-1} less stable

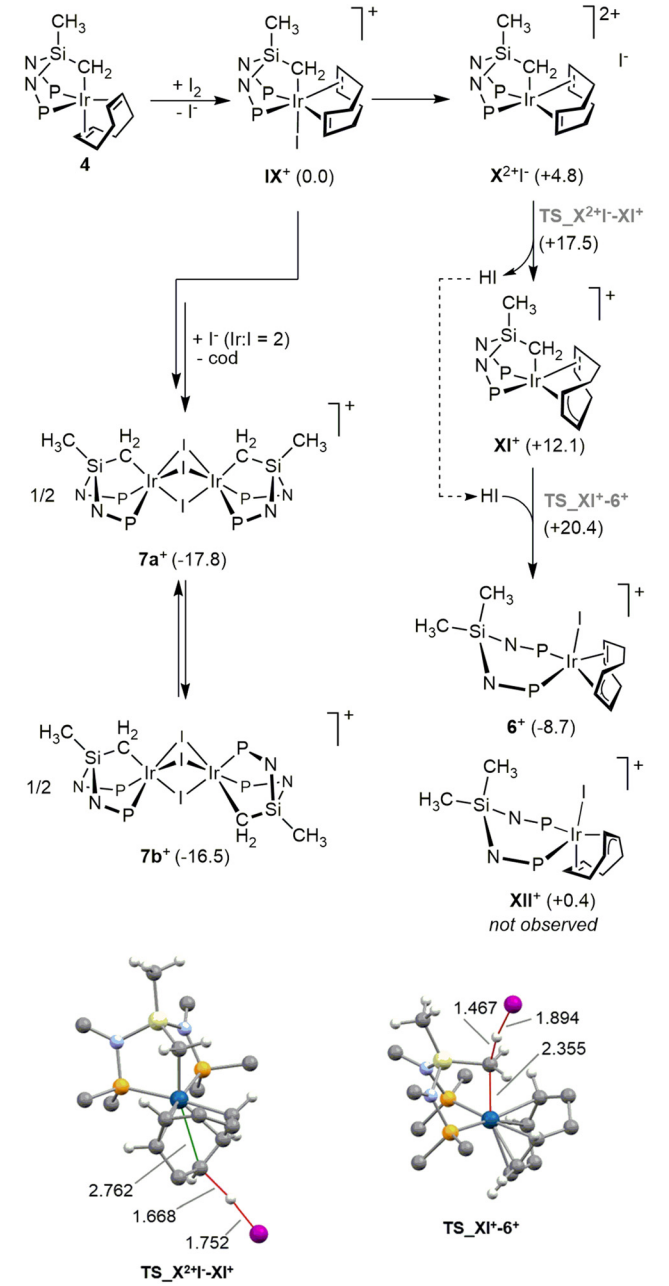

Scheme 8 (Top) Reaction sequences for the formation of **7a** + **7b**$^+$ (left) and **6**$^+$ (right) with relative Gibbs free energy of intermediates (kcal mol^{-1}, B97D3/def2svp). (Bottom) Calculated structures of the transition states **TS_X^{2+}I$^-$-XI$^+$** and **TS_XI$^+$-6$^+$** along with selected interatomic distances (Å). Gray, carbon; white, hydrogen; violet, nitrogen; yellow, silicon; orange, phosphorus; blue, iridium; purple, iodine.

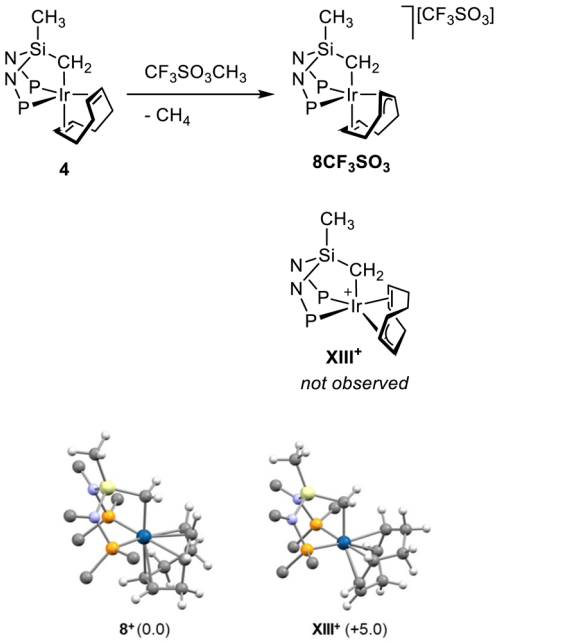

Scheme 9 (Top) Synthesis of [Ir{κ^3*C*,*P*,*P*′-(SiNP-H)}(η^2,η^3-C_8H_{11})][CF_3SO_3] (**8**CF_3SO_3). (Bottom) Calculated structures for **8**$^+$ and **XIII**$^+$ along with relative Gibbs free energy (kcal mol^{-1}, B97D3/def2svp). For clarity, only *ipso* atoms of phenyl and tolyl groups are shown. Gray, carbon; white, hydrogen; violet, nitrogen; yellow, silicon; orange, phosphorus, blue, iridium.

than $\mathbf{6}^+$, which rules out its presence in solution in agreement with the observed NMR spectra.

The reaction of **4** with methyl triflate also resulted in the formal two-electron oxidation of iridium. As a matter of fact, upon reaction of **4** with methyl triflate (1 : 1) for 4 days at room temperature, [Ir{κ^3*C*,*P*,*P*′-(SiNP-H)}(η^2,η^3-C_8H_{11})][CF_3SO_3] (**8**CF_3SO_3) forms along with methane (observed *via* both GC and ^{1}H NMR spectroscopy) as a consequence of the unusual hydride abstraction from the cod ligand (Scheme 9). $\mathbf{8}^+$ contains the iridium(III)-κ^3*C*,*P*,*P*′-(SiNP-H) platform and the cycloocta-2,6-dien-1-yl ligand (C_8H_{11}) exhibiting a η^2,η^3 coordination. The ^{1}H and ^{31}P{^{1}H} NMR spectra indicate that the κ^3*C*, *P*,*P*′ coordination of the ligand SiNP-H is preserved and experiments a non-symmetric environment. Actually, two ^{31}P{^{1}H} signals (35.4, 31.5 ppm; $^2J_{PP}$ = 9.2 Hz) are observed along with two ^{1}H multiplets for the non-equivalent hydrogen atoms of the methylene group $IrCH_2Si$ (0.55, 0.46 ppm, δ_C −13.8 ppm). Fig. 10 (top) shows a selection of ^{1}H and ^{13}C{^{1}H} NMR data for the ligand C_8H_{11} of $\mathbf{8}^+$. It is worth a mention that the putative isomer $\mathbf{XIII}^+$ exhibiting the olefinic group at one of the coordination sites *trans* to phosphorus and the allyl moiety formally spanning the remaining sites *trans* to phosphorus and *trans* to CH_2 was not observed (Scheme 9). Actually, confirming the proposed structure for $\mathbf{8}^+$, $\mathbf{XIII}^+$ was calculated to be 5 kcal mol^{-1} less stable than $\mathbf{8}^+$ (Scheme 9).

The mechanism of the formation of $\mathbf{6}^+$ was explored by means of DFT calculations showing that it consists of a straightforward hydride abstraction from the coordinated cod promoted by methyl triflate, ultimately acting as an electrophile (Fig. 10), and goes through the transition state **TS_4-8**$^+$ (+28.9 kcal mol^{-1}).

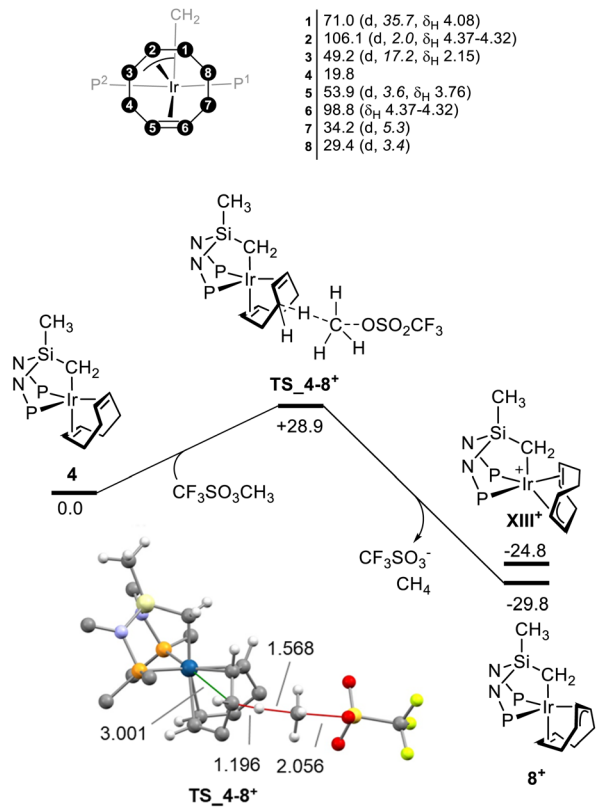

Fig. 10 (Top) Selected NMR data for $\mathbf{8}^+$ [δ_C, along with J_{CP}, italics, and δ_H]. (Bottom) Gibbs free energy profile for the reaction of **4** with methyl triflate (kcal mol^{-1}, B97D3/def2svp) along with the calculated structure of **TS_4-8**$^+$ and selected interatomic distances (Å). Gray, carbon; white, hydrogen; violet, nitrogen; red, oxygen; pale green, fluorine; yellow, silicon; orange, phosphorus; dark yellow, sulphur; blue, iridium.

Conclusions

The iridium(I)-aminophoshane derivative [IrCl(cod)(SiNP)] is a versatile precursor for the preparation of a range of iridium(III) complexes with the SiNP ligand coordinated either κ^2*P*,*P*′ or κ^3*C*,*P*,*P*′. The oxidative addition of allyl chloride to [IrCl(cod)(SiNP)] affords the thermally stable [$IrCl_2$(η^3-C_3H_5)(SiNP)] (**1**) which, in turn, reacts with *tert*-butyl isocyanide rendering the substitution product [IrCl(η^3-C_3H_5)(CN^{t}Bu)(SiNP)]Cl (**2**Cl). The observed intermediate [$IrCl_2$(η^1-C_3H_5)(CN^{t}Bu)(SiNP)] (**3**) as well as DFT calculations point out that the mechanism is associative. In this connection, the $\eta^3 \rightleftarrows \eta^1$ haptotropic shift of the allyl ligand is key for the outcome of the reaction.

The iridium(I) pentacoordinate [Ir{κ^3*C*,*P*,*P*′-(SiNP-H)}(cod)] (**4**) is smoothly obtained treating [IrCl(cod)(SiNP)] with potassium acetate *via* an outer sphere mechanism in which the acetate ion deprotonate the $SiCH_3$ group while the carbon–iridium bond forms. The two-electron oxidation of [Ir{κ^3*C*,*P*,*P*′-(SiNP-H)}(cod)] (**4**) gives rise to a variety of iridium(III) derivatives. The reaction of **4** with ferrocenium in acetonitrile leads to the oxidation of iridium(I) to iridium(III) rendering the octahedral cation [Ir{κ^3*C*,*P*,*P*′-(SiNP-H)}(CH_3CN)$_3$]$^{2+}$ ($\mathbf{5}^{2+}$) as a result of the substitution of the cod ligand by three acetonitrile ligands. Alternatively, I_2 readily oxidises **4** yielding a mixture of iridium(III) complexes as a consequence of either cod activation or cod substitution, namely [IrI(κ^2*P*,*P*′-SiNP)(η^2,η^3-C_8H_{11})]$^+$ ($\mathbf{6}^+$) and [Ir_2{κ^3*C*,*P*,*P*′-(SiNP-H)}$_2$(μ-I)$_3$]$^+$ ($\mathbf{7a}^+$/$\mathbf{7b}^+$), respectively. As a matter of fact, once [Ir{κ^3*C*,*P*,*P*′-(SiNP-H)}(cod)] is oxidised, I^- is able to either displace cod affording dinuclear species $\mathbf{7a}^+$/$\mathbf{7b}^+$ or shuttle one H^+ ion from cod to the κ^3*C*,*P*,*P*′-(SiNP-H) ligand in a step-wise fashion, eventually affording the iridium(III) complex $\mathbf{6}^+$. Finally, methyl triflate is also able to oxidise **4** affording $\mathbf{8}^+$ as a result of the hydride abstraction from the cod ligand.

Experimental

General section

All the operations were carried out using standard Schlenk tube techniques under an atmosphere of pre-purified argon or in a Braun glove-box under argon. Solvents were dried and purified according to standard procedures and distilled under argon, or obtained oxygen-and water-free from a solvent purification system (Innovative Technologies). The compounds $SiMe_2${N(4-$C_6H_4CH_3$)(PPh_2)}$_2$ (SiNP)[6] and [IrCl(cod)(SiNP)][7a]

were prepared according to the literature. NMR spectra were recorded with Bruker spectrometers (AV300, AV400, or AV500) and are referred to $SiMe_4$ (^1H, ^{13}C), and H_3PO_4 (^{31}P). The proposed ^1H, ^{13}C, and ^{31}P assignment relies on the combined analysis of 1D [^1H, $^1H\{^{31}P\}$, $^{13}C\{^1H\}$-apt, $^{31}P\{^1H\}$] and 2D NMR spectra (^1H–^1H COSY, ^1H–^1H NOESY, ^1H–^{13}C HSQC, ^1H–^{13}C HMBC, ^1H–^{31}P HMBC). Fig. 11 shows the numbering scheme used for the assignment of NMR signals in **1**, **2**Cl, **6**I, and **8**CF_3SO_3. Whenever labels P^1 and P^2, are used for non-equivalent phosphorus atoms, superscript labels "tol-P1/2" and "PhP1/2" are used for hydrogen and carbon atoms belonging to the tolyl and phenyl groups attached/linked to the phosphorus atom P^1/P^2, respectively.

MALDI-TOF mass spectra were recorded using a Bruker AutoFLEX III-TOF/TOF using *trans*-2-[3-(4-*tert*-butylphenyl)-2-methyl-2-propenylidene]malononitrile (DCTB) as a matrix.

Synthesis of [$IrCl_2(\eta^3$-$C_3H_5)(\kappa^2$*P,P′*-SiNP)] (1). A dichloromethane suspension (10 mL) of [IrCl(cod)(SiNP)] (242 mg, 0.248 mmol, 974.64 g mol^{-1}) was added with allyl chloride (20.2 μL, 0.248 mmol, 76.52 g mol^{-1}, 0.939 g mL^{-1}). The light yellow resulting suspension was stirred at 313 K for 6 h, evaporated up to 5 mL and added with hexane (5 mL), affording a light yellow solid which was filtered off, washed with hexane, dried *in vacuo* and finally identified as [$IrCl_2(\eta^3$-$C_3H_5)(\kappa^2$*P,P′*-SiNP)] (**1**, 227 mg, 97% yield). Found: C 54.69, H 4.78, N 3.01. Calcd for $C_{43}H_{45}Cl_2IrN_2P_2Si$ (942.99 g mol^{-1}): C 54.77, H 4.81, N 2.97. ^1H NMR (CD_2Cl_2, 298 K): δ_H 8.26–7.71 (7H tot; 4H, *o*-PPh; 2H, *m*-PPh; 1H, *p*-PPh), 7.53 (br, 2H, *m*-PPh), 7.43–7.26 (4H tot; 2H, *o*-PPh; 1H, *p*-PPh; 1H, $C^2H^{tol\text{-}P2}$), 7.24–6.94 (10H tot; 2H, *o*-PPh; 4H, *m*-PPh; 2H, *p*-PPh; 1H, $C^2H^{tol\text{-}P1}$; 1H, $C^3H^{tol\text{-}P1}$), 6.80 (d, 1H, $^3J_{HH}$ = 8.2 Hz, $C^3H^{tol\text{-}P2}$), 6.67–6.51 (3H tot; 1H, $C^2H^{tol\text{-}P2}$; 1H, $C^3H^{tol\text{-}P1}$; 1H, $C^3H^{tol\text{-}P2}$), 5.48 (d, 1H, $^3J_{HH}$ = 8.2 Hz, $C^2H^{tol\text{-}P1}$), 4.86 (m, 1H, C^2H^{all}), 4.16–4.03 (2H tot; 1H, $C^1H_a^{all}$; 1H, $C^1H_b^{all}$), 2.21 (s, 3H, $CH_3^{tol\text{-}P1}$), 2.14 (m, 1H, $C^3H_b^{all}$), 2.08 (s, 3H, $CH_3^{tol\text{-}P2}$), 1.49 (br, 1H, $C^3H_a^{all}$), 0.88 (s, 3H, $SiCH_3^b$), −0.28 (s, 3H, $SiCH_3^a$). $^{31}P\{^1H\}$ NMR (CD_2Cl_2, 298 K): δ_P 30.6 (d, 1P, $^2J_{PP}$ = 25.2 Hz, $SiNP^1$), 24.3 (d, 1P, $^2J_{PP}$ = 25.2 Hz, $SiNP^2$). ^1H NMR (CD_2Cl_2, 233 K): δ_H 9.59 (br, 1H, *o*-PPh), 8.75 (dd, 1H, $^3J_{HP}$ = 11.5 Hz, $^3J_{HH}$ = 7.4 Hz, *o*-PPh), 8.04–7.59 (5H tot; 2H, *o*-PPh; 2H, *m*-PPh; 1H, *p*-PPh), 7.53 (t, 2H, $^3J_{HH}$ = 7.1 Hz, *m*-PPh), 7.36–7.25 (2H tot; 1H, *p*-PPh; 1H, $C^2H^{tol\text{-}P2}$), 7.18 (t, 2H, $^3J_{HH}$ = 7.4 Hz, *o*-PPh), 7.15–7.08 (3H tot; 2H, *m*-PPh; 1H, $C^2H^{tol\text{-}P1}$), 7.07–6.98 (3H tot, 2H, *p*-PPh; 1H, $C^3H^{tol\text{-}P1}$), 6.88 (m, 2H, *m*-PPh), 6.79 (d, 1H, $^3J_{HH}$ = 7.9 Hz, $C^3H^{tol\text{-}P2}$), 6.67–6.51 (5H tot; 2H, *o*-PPh; 1H, $C^2H^{tol\text{-}P2}$; 1H, $C^3H^{tol\text{-}P1}$; 1H, $C^3H^{tol\text{-}P2}$), 5.32 (d, 1H, $^3J_{HH}$ = 7.9 Hz, $C^2H^{tol\text{-}P1}$), 4.84 (m, 1H, C^2H^{all}), 4.03 (m, 1H, $C^1H_a^{all}$), 3.94 (dd, $^3J_{HH}$ = 12.6 Hz, $^3J_{HP}$ = 7.4 Hz 1H, $C^1H_b^{all}$), 2.17 (s, 3H, $CH_3^{tol\text{-}P1}$), 2.06 (br, 1H, $C^3H_b^{all}$), 2.03 (s, 3H, $CH_3^{tol\text{-}P2}$), 1.43 (br, 1H, $C^3H_a^{all}$), 0.83 (s, 3H, $SiCH_3^b$), −0.35 (s, 3H, $SiCH_3^a$). $^{13}C\{^1H\}$ NMR (CD_2Cl_2, 233 K): δ_C 138.6 (d, $^2J_{CP}$ = 10.2 Hz, $C^{1,\ tol\text{-}P1}$), 138.0 (d, $^2J_{CP}$ = 7.3 Hz, $C^{1,\ tol\text{-}P2}$), 137.1 ($C^{2,\ PhP}$), 136.9 (d, $^5J_{CP}$ = 1.1 Hz, $C^{4,\ tol\text{-}P1}$), 135.9 (d, $^5J_{CP}$ = 2.2 Hz, $C^{4,\ tol\text{-}P2}$), 135.4 (d, $^1J_{CP}$ = 68.3 Hz, $C^{1,\ PhP}$), 134.8 (d, $^1J_{CP}$ = 59.4 Hz, $C^{1,\ PhP}$), 134.77 (d, $^1J_{CP}$ = 60.1, Hz, $C^{1,\ PhP}$), 134.75 (d, $^1J_{CP}$ = 60.7, Hz, $C^{1,\ PhP}$), 133.9 ($C^{2,\ tol\text{-}P2}$), 132.8 ($C^{2,\ PhP}$), 132.3 (d, $^4J_{CP}$ = 1.6 Hz, $C^{4,\ PhP}$), 132.1 (d, $^4J_{CP}$ = 1.1 Hz, $C^{4,\ PhP}$), 131.9 ($C^{3,\ PhP}$), 131.3 ($C^{2,\ PhP}$), 131.0 ($C^{3,\ PhP}$), 130.7 ($C^{3,\ tol\text{-}P1}$), 129.3 ($C^{3,\ tol\text{-}P2}$, $C^{3,\ tol\text{-}P1}$, $C^{2,\ tol\text{-}P1}$, $C^{3,\ PhP}$), 128.8 ($C^{2,\ tol2}$), 128.1 ($C^{4,\ PhP}$), 127.0 ($C^{3,\ PhP}$), 125.7 ($C^{4,\ PhP}$), 102.9 ($C^{2,\ all}$), 72.1 (d, $^2J_{CP}$ = 30.5 Hz, $C^{1,\ all}$), 43.2 ($C^{3,\ all}$), 21.0 ($CH_3^{tol\text{-}P1}$), 20.9 ($CH_3^{tol\text{-}P2}$), 2.7 (d, $^3J_{CP}$ = 2.3 Hz, $SiCH_3^a$), 2.4 ($SiCH_3^b$). $^{31}P\{^1H\}$ NMR (CD_2Cl_2, 233 K): δ_P 30.2 (d, 1P, $^2J_{PP}$ = 25.8 Hz, $SiNP^1$), 23.8 (d, 1P, $^2J_{PP}$ = 25.8 Hz, $SiNP^2$).

Synthesis of [$IrCl(\eta^3$-$C_3H_5)(CN^tBu)(\kappa^2$*P,P′*-SiNP)]Cl (2Cl). A toluene suspension (15 mL) of [$IrCl_2(\eta^3$-$C_3H_5)(\kappa^2$*P,P′*-SiNP)] (**1**, 114 mg, 0.121 mmol, 942.99 g mol^{-1}) was added with CN^tBu (13.7 μL, 0.121 mmol, 83.13 g mol^{-1}, 0.735 g mL^{-1}). The resulting light yellow suspension was stirred for 24 h, evaporated up to 5 mL and added with hexane (5 mL). The resulting colourless solid was filtered off, washed with hexane, dried *in vacuo* and finally identified as [$IrCl(\eta^3$-$C_3H_5)(CN^tBu)(\kappa^2$*P,P′*-SiNP)]Cl (**2**Cl, 85.4 mg, 69% yield). Found: C 56.25, H 5.25, N 4.18. Calcd for $C_{48}H_{54}Cl_2IrN_3P_2Si$ (1026.12 g mol^{-1}): C 56.18; H, 5.30; N, 4.10. ^1H NMR ($CDCl_3$, 298 K): δ_H 8.03 (m, 1H, *p*-P^1Ph), 7.92 (dt, 2H, $^3J_{HH}$ = 7.5, $^3J_{HP}$ = 3.3 *m*-P^1Ph), 7.85 (m, 2H, *o*-P^1Ph), 7.67 (m, 2H, *o*-P^2Ph), 7.57 (t, 1H, $^3J_{HH}$ = 7.3 *p*-P^2Ph), 7.47–6.99 (15H tot; 2H, *o*-P^1Ph; 2H, *o*-P^2Ph; 2H, *m*-P^1Ph, 4H, *m*-P^2Ph; 1H, *p*-P^1Ph; 1H, *p*-P^2Ph; 1H, $C^2H^{tol\text{-}P1}$; 1H, $C^2H^{tol\text{-}P2}$; 1H, $C^3H^{tol\text{-}P2}$), 6.78 (d, 1H, $^3J_{HH}$ = 8.3 Hz $C^3H^{tol\text{-}P1}$), 6.66 (d, 1H, $^3J_{HH}$ = 8.3 Hz, $C^3H^{tol\text{-}P1}$), 6.62 (d, 1H, $^3J_{HH}$ = 8.2 Hz, $C^3H^{tol\text{-}P2}$), 6.47 (d, 1H, $^3J_{HH}$ = 8.2 Hz, $C^2H^{tol\text{-}P2}$), 5.43 (d, 1H, $^3J_{HH}$ = 8.3 Hz, $C^2H^{tol\text{-}P1}$), 4.89 (m, 1H, C^2H^{all}), 3.86 (dd, 1H, $^3J_{HH}$ = 7.7 Hz, $^3J_{HP}$ = 4.6 Hz, $C^1H_b^{all}$), 3.72 (dd, 1H, $^3J_{HH}$ = 12.6 Hz, $^3J_{HP}$ = 7.1 Hz, $C^1H_a^{all}$), 2.31 (d, 1H, $^3J_{HH}$ = 20.3 Hz, $C^3H_b^{all}$), 2.19 (s, 3H, $CH_3^{tol\text{-}P2}$), 2.13–1.97 (12H tot; 9H, CN^tBu; 3H, $CH_3^{tol\text{-}P2}$) 2.00 (br, 1H, $C^3H_a^{all}$), 0.58 (s, 3H, $SiCH_3$), −0.33 (s, 3H, $SiCH_3$). $^{13}C\{^1H\}$ NMR ($CDCl_3$, 298 K): δ_C 138.1 (d, $^5J_{CP}$ = 2.2 Hz, $C^{4,\ tol\text{-}P2}$), 137.7 (d, $^5J_{CP}$ = 2.5 Hz, $C^{4,\ tol\text{-}P1}$), 137.43 (d, $^2J_{CP}$ = 9.4 Hz, $C^{1,\ tol\text{-}P2}$), 137.41 (d, $^2J_{CP}$ = 7.8 Hz, $C^{1,\ tol\text{-}P1}$), 135.9 (d, $^2J_{CP}$ = 10.1 Hz, $C^{2,\ PhP\text{-}P2}$), 135.0 (d, $^1J_{CP}$ = 68.6 Hz, $C^{1,\ PhP\text{-}P1}$), 133.6 ($C^{4,}$

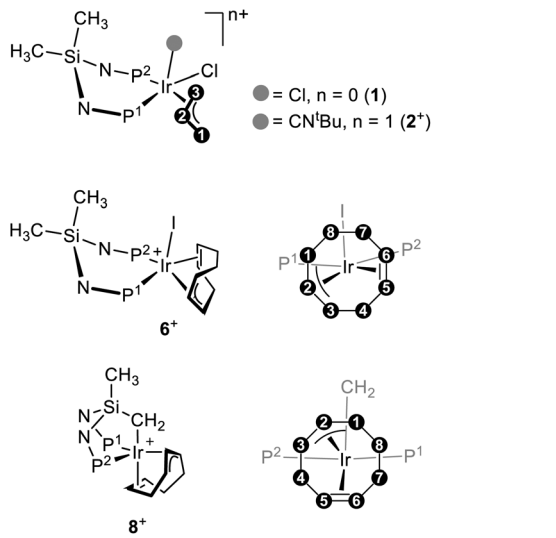

Fig. 11 Numbering scheme for the assignment of NMR signals for **1**, $\mathbf{2}^+$, $\mathbf{6}^+$, and $\mathbf{8}^+$.

^{PhP1}) 133.5 (d, $^{2}J_{CP}$ = 8.4 Hz, $C^{2,\ PhP1}$), 133.2 (d, $^{2}J_{CP}$ = 9.3 Hz, $C^{2,\ PhP2}$), 133.1 (d, $^{4}J_{CP}$ = 2.4 Hz, $C^{4,\ PhP2}$), 132.4 ($C^{4,\ PhP1}$), 132.2 ($C^{4,\ PhP2}$), 131.8 (d, $^{3}J_{CP}$ = 2.3 Hz, $C^{2,\ tol\text{-}P1}$), 131.5 (d, $^{3}J_{CP}$ = 2.5 Hz, $C^{2,\ tol\text{-}P1}$), 131.1 (d, $^{1}J_{CP}$ = 64.8 Hz, $C^{1,\ PhP2}$), 131.0 ($C^{3,\ tol\text{-}P2}$), 130.9 (d, $^{2}J_{CP}$ = 8.3 Hz, $C^{2,\ PhP\text{-}P1}$), 130.43 (d, $^{4}J_{CP}$ = 3.5 Hz, $C^{3,\ tol\text{-}P1}$), 130.39 (d, $^{4}J_{CP}$ = 5.4 Hz, $C^{3,\ tol\text{-}P2}$), 130.0 (d, $^{3}J_{CP}$ = 3.0 Hz, $C^{2,\ tol\text{-}P2}$), 129.9 (d, $^{3}J_{CP}$ = 1.9 Hz, $C^{2,\ tol\text{-}P2}$), 129.9 (d, $^{3}J_{CP}$ = 10.7 Hz, $C^{3,\ PhP1}$), 129.2 ($C^{3,\ tol\text{-}P1}$), 128.63 (d, $^{3}J_{CP}$ = 11.3 Hz, $C^{3,\ PhP2}$), 127.6 (d, $^{3}J_{CP}$ = 11.6 Hz, $C^{3,\ PhP1}$), 127.4 (d, $^{3}J_{CP}$ = 11.5 Hz, $C^{3,\ PhP2}$), 108.3 ($C^{2,\ all}$), 63.6 (d, $^{2}J_{CP}$ = 28.6 Hz, $C^{1,\ all}$), 60.1 ($C^{3,\ all}$), 31.0 ($CH_3CN^{t}Bu$), 21.1 ($CH_3^{tol\text{-}P2}$), 21.0 ($CH_3^{tol\text{-}P1}$), 3.3 (CH_3Si^{down}), 2.9 (d, $^{3}J_{CP}$ = 2.7 Hz, CH_3Si^{up}). $^{31}P\{^{1}H\}$ NMR ($CDCl_3$, 298 K): δ_P 28.3 (d, 1P, $^{2}J_{PP}$ = 20.9 Hz, $SiNP^{1}$), 25.9 (d, 1P, $^{2}J_{PP}$ = 20.9 Hz, $SiNP^{2}$).

Synthesis of $[IrCl_2(\eta^1\text{-}C_3H_5)(CN^tBu)(\kappa^2P,P'\text{-SiNP})]$ (3). A toluene suspension (10 mL) of $[IrCl_2(\eta^3\text{-}C_3H_5)(\kappa^2P,P'\text{-SiNP})]$ (**1**, 83.6 mg, 88.7 μmol, 942.99 g mol^{-1}) was added with CN^tBu (10.0 μL, 88.4 μmol, 83.13 g mol^{-1}, 0.735 g mL^{-1}). After 1 h stirring, the resulting light yellow suspension was evaporated up to 5 mL and added with hexane (5 mL). The resulting colourless solid was filtered off, washed with hexane, dried *in vacuo* and finally identified as a mixture of **1** and $[IrCl_2(\eta^1\text{-}C_3H_5)(CN^tBu)(\kappa^2P,P'\text{-SiNP})]$ (**3**) (**3** : **1** = 4 : 1, 60.1 mg). NMR data for **3**: ^{1}H NMR (CD_2Cl_2, 233 K): δ_H 7.62 (m, 4H, *o*-PPh), 7.49–7.33 (10H tot: 4H, *o*-PPh; 4H, *m*-PPh, 2H, *p*-PPh), 7.25 (t, 2H, $^{3}J_{HH}$ = 7.2 Hz, *p*-PPh), 7.10 (t, 4H, $^{3}J_{HH}$ = 7.2 Hz, *m*-PPh), 6.74–6.68 (5H tot: 1H, C^2H^{all}, 2H, C^2H^{tol}; 2H, C^3H^{tol}), 6.59 (d, 2H, $^{3}J_{HH}$ = 8.2 Hz, C^3H^{tol}), 6.34 (d, 2H, $^{3}J_{HH}$ = 8.2 Hz, C^2H^{tol}), 5.18 (d, 1H, $^{3}J_{HH\ trans}$ = 17.1 Hz, $C^3H^{all\ trans}$), 5.03 (d, 1H, $^{3}J_{HH\ cis}$ = 9.7 Hz, $C^3H^{all\ cis}$), 3.34 (br, 2H, C^1H^{all}), 2.09 (s, 6H, CH_3^{tol}), 1.06 (s, 9H, CN^tBu), 0.47 (s, 3H, CH_3Si), −0.05 (s, 3H, CH_3Si); $^{13}C\{^{1}H\}$ NMR (CD_2Cl_2, 233 K): δ_C 148.2 ($C^{2,\ all}$), 138.6 (t, $^{3}J_{CP}$ = 4.3 Hz, $C^{1,\ tol}$), 136.7 (t, $^{2}J_{CP}$ = 4.4 Hz, $C^{2,\ PhP}$), 136.5 ($C^{4,\ tol}$), 133.4 ($C^{2,\ tol}$), 133.1 (t, $^{2}J_{CP}$ = 4.1 Hz, $C^{2,\ PhP}$), 132.3 ($C^{2,\ tol}$), 130.7 ($C^{2,\ PhP}$), 130.5 ($C^{2,\ PhP}$), 129.1 ($C^{3,\ tol}$), 127.4 (t, $^{3}J_{CP}$ = 5.4 Hz, $C^{3,\ PhP}$), 126.0 (t, $^{3}J_{CP}$ = 5.4 Hz, $C^{3,\ PhP}$), 108.3 ($C^{3,\ all}$), 56.9 ($\underline{C}N^tBu$), 29.5 ($CH_3^{CN^tBu}$), 20.9 (CH_3^{tol}), 5.28 ($C^{1,\ all}$), 4.5 (CH_3Si), 3.4 (CH_3Si); $^{31}P\{^{1}H\}$ NMR (CD_2Cl_2, 233 K): δ_P 31.9 (2P, SiNP).

Synthesis of $[Ir\{\kappa^3C,P,P'\text{-(SiNP-H)}\}(cod)]$ (4). A dichloromethane suspension (8 mL) of [IrCl(cod)(SiNP)] (180 mg, 0.185 mmol, 974.64 g mol^{-1}) was added with potassium acetate (21.7 mg, 0.221 mmol, 98.14 g mol^{-1}). After 20 h stirring, the resulting suspension was filtered, evaporated up to 2 mL and added with hexane (5 mL) affording a light yellow solid which was filtered off, washed with hexane, dried *in vacuo* and finally identified as $[Ir\{\kappa^3C,P,P'\text{-(SiNP-H)}\}(cod)]$ (**4**, 138 mg, 80% yield). Found: C 61.69, H 5.31, N 3.15. Calcd for $C_{48}H_{51}IrN_2P_2Si$ (938.18 g mol^{-1}): C 61.45, H 5.48, N 2.99. ^{1}H NMR (CD_2Cl_2, 298 K): δ_H 7.59 (m, 4H, *o*-PPh), 7.42–7.27 (8H tot; 4H, *m*-PPh, 4H, *p*-PPh), 7.08 (t, 4H, $^{3}J_{HH}$ = 7.3 Hz, *m*-PPh), 7.95 (m, 4H, *o*-PPh), 6.82 (d, 4H, $^{3}J_{HH}$ = 8.1 Hz, C^3H^{tol}), 6.57 (d, 4H, $^{3}J_{HH}$ = 8.1 Hz, C^2H^{tol}), 3.60 (br, 2H, $C^{sp2}H^{cod}$), 2.60 (br, 2H, $C^{sp2}H^{cod}$), 2.21 (s, 6H, CH_3^{tol}), 2.03–1.62 (m, 8H, $C^{sp3}H^{cod}$), 0.14 (t, 2H, $^{3}J_{HP}$ = 9.3 Hz, $SiCH_2Ir$), −0.83 (s, 3H, $SiCH_3$). $^{13}C\{^{1}H\}$ NMR (CD_2Cl_2, 298 K): δ_C 143.4 (t, $^{2}J_{CP}$ = 5.8 Hz, $C^{1,\ tol}$), 136.4 (dd, $^{1}J_{CP}$ = 47.8 Hz, $^{3}J_{CP}$ = 7.8 Hz, $C^{1,\ PhP1}$), 135.2 (t, $^{2}J_{CP}$ = 6.3, $C^{2,\ PhP}$), 134.8 ($C^{4,\ tol}$), 133.4 (dd, $^{2}J_{CP}$ = 6.8 Hz, $C^{2,\ PhP}$), 130.7 ($C^{2,\ tol}$), 129.9 ($C^{4,\ PhP}$), 129.5 ($C^{4,\ PhP}$), 127.9 ($C^{3,\ PhP}$), 76.0 ($C^{sp2\ cod}$), 56.8 (dd, $^{3}J_{CP}$ = 42.7 Hz, $^{3}J_{CP}$ = 16.7 Hz, $C^{sp2\ cod}$), 34.7 ($C^{sp3\ cod}$), 33.8 ($C^{sp3\ cod}$), 21.3 (CH_3^{tol}), −0.06 (t, $^{3}J_{CP}$ = 7.5 Hz, CH_3Si), −14.7 (t, $^{2}J_{CP}$ = 4.2 Hz, CH_2Si). $^{31}P\{^{1}H\}$ NMR (CD_2Cl_2, 298 K): δ_P 47.1 (s, SiNP).

Synthesis of $[Ir\{\kappa^3C,P,P'\text{-(SiNP-H)}\}(CH_3CN)_3][PF_6]_2$ (5$[PF_6]_2$). An acetonitrile suspension (10 mL) of $[Ir\{\kappa^3C,P,P'\text{-(SiNP-H)}\}(cod)]$ (**4**, 112 mg, 0.119 mmol, 938.18 g mol^{-1}) was added with ferrocenium hexafluorophosphate (79.1 mg, 0.239 mmol, 331.00 g mol^{-1}). After 2 h stirring, the resulting orange solution was evaporated up to 4 mL and added with hexane (5 mL) affording a colorless solid which was filtered off, washed with diethyl ether (3 × 5 mL), dried *in vacuo* and finally identified as $[Ir\{\kappa^3C,P,P'\text{-(SiNP-H)}\}(CH_3CN)_3][PF_6]_2$ (5$[PF_6]_2$, 105 mg, 71% yield). Found: C 44.62, H 3.92, N 5.59. Calcd for $C_{46}H_{48}F_{12}IrN_5P_4Si$ (1243.09 g mol^{-1}): C 44.45, H 3.89, N 5.63. ^{1}H NMR (CD_2Cl_2, 298 K): δ_H 7.62 (12H tot, 4H, *o*-PPh; 4H, *m*-PPh; 4H, *p*-PPh), 7.24 (t, 4H, $^{3}J_{HH}$ = 7.8 Hz, *m*-PPh), 7.10 (dd, 4H, $^{3}J_{HP}$ = 11.8 Hz, $^{3}J_{HH}$ = 7.8 Hz, *o*-PPh), 6.92 (d, 4H, $^{3}J_{HH}$ = 8.2 Hz, C^3H^{tol}), 6.52 (d, 4H, $^{3}J_{HH}$ = 8.2 Hz, C^2H^{tol}), 2.44 (s, 3H, CH_3CN^{ax}), 2.24 (s, 6H, CH_3^{tol}), 1.98 (s, 6H, CH_3CN^{eq}), 1.46 (t, $^{3}J_{HP}$ = 1.6 Hz, 2H, $SiCH_2Ir$), 0.36 (s, 3H, $SiCH_3$). $^{13}C\{^{1}H\}$ NMR (CD_2Cl_2, 298 K): δ_C 137.3 ($C^{4,\ tol}$), 137.2 (t, $^{2}J_{CP}$ = 4.3 Hz, $C^{1,\ tol}$), 134.5 (t, $^{2}J_{CP}$ = 5.3, $C^{2,\ PhP}$), 133.6 ($C^{4,\ PhP}$), 133.2 ($C^{4,\ PhP}$), 133.04 (t, $^{2}J_{CP}$ = 4.9 Hz, $C^{2,\ PhP}$), 131.6 (d, $^{1}J_{CP}$ = 65.5, $C^{2,\ PhP}$), 130.8 ($C^{3,tol}$), 129.8 (t, $^{3}J_{CP}$ = 5.8, $C^{3,\ PhP}$), 129.3 (t, $^{3}J_{CP}$ = 5.9, $C^{3,\ PhP}$), 129.01 (t, $^{3}J_{CP}$ = 2.0, $C^{2,\ tol}$), 126.6 (d, $^{1}J_{CP}$ = 70.2 Hz, $C^{1,\ PhP}$), 122.8 ($CH_3\underline{C}N^{ax}$), 121.7 (t, $^{3}J_{CP}$ = 9.7, $CH_3\underline{C}N^{eq}$), 21.2 (CH_3^{tol}), 3.9 ($\underline{C}H_3CN^{ax}$), 3.2 ($\underline{C}H_3CN^{eq}$), −1.32 (t, $^{3}J_{CP}$ = 6.8 Hz, CH_3Si), −19.6 (t, $^{2}J_{CP}$ = 4.0 Hz, CH_2Si). $^{31}P\{^{1}H\}$ NMR (CD_2Cl_2, 298 K): δ_P 18.2 (2P, SiNP), −145.5 (hept, 2P, $^{1}J_{PF}$ = 710.8 Hz, PF_6^-).

Synthesis of $[Ir\{\kappa^3C,P,P'\text{-(SiNP-H)}\}(CH_3CN)_3][CF_3SO_3]_2$ (5$[CF_3SO_3]_2$). An acetonitrile suspension (10 mL) of $[Ir\{\kappa^3C,P,P'\text{-(SiNP-H)}\}(cod)]$ (**4**, 304 mg, 0.324 mmol, 938.18 g mol^{-1}) was added with ferrocenium triflate (217 mg, 0.648 mmol, 335.10 g mol^{-1}). The work up was similar to that described for 5$[PF_6]_2$, yielding $[Ir\{\kappa^3C,P,P'\text{-(SiNP-H)}\}(CH_3CN)_3][CF_3SO_3]_2$ as a colourless solid (5$[CF_3SO_3]_2$, 303 mg, 75% yield). Found: C 45.99, H 3.92, N 5.55. Calcd for $C_{48}H_{48}F_6IrN_5O_6P_2S_2Si$ (1251.30 g mol^{-1}): C 46.07, H 3.87, N 5.60. ^{1}H, $^{1}H\{^{31}P\}$ and $^{31}P\{^{1}H\}$ NMR of 5$[CF_3SO_3]_2$ are similar to those given for 5$[PF_6]_2$.

Reaction of $[Ir\{\kappa^3C,P,P'\text{-(SiNP-H)}\}(cod)]$ with I_2. A dichloromethane solution (10 mL) of $[Ir\{\kappa^3C,P,P'\text{-(SiNP-H)}\}(cod)]$ (**4**, 121 mg, 0.129 mmol, 938.18 g mol^{-1}) was added with I_2 (32.7 mg, 0.129 mmol, 253.81 g mol^{-1}) at 233 K. The resulting yellow solution was stirred for 30 min, evaporated up to 3 mL and added with hexane (5 mL) affording an orange solid which was filtered off, washed with hexane, dried *in vacuo* finally identified as a mixture of $[IrI(\eta^2,\eta^3\text{-}C_8H_{11})(\kappa^2P,P'\text{-SiNP})]I$ (**6I**) and $[Ir_2\{\kappa^3C,P,P'\text{-(SiNP-H)}\}_2(\mu\text{-}I)_3]I$ (**7aI** + **7bI**) and (110 mg, **6I** : **7aI** : **7bI** = 54 : 33 : 13, ^{31}P). A small amount (22 mg) of analytically and spectroscopically pure **6I** was recovered by crystallization in acetonitrile/Et_2O. Found: C 48.89, H 4.32, N 2.29.

Calcd for $C_{48}H_{51}I_2IrN_2P_2Si$ (1191.99 g mol^{-1}): C 48.37, H 4.31, N 2.35. ^{1}H NMR (CD_2Cl_2, 298 K): δ_H 8.08–7.83 (br, 4H tot; 2H, *o*-P^{1}Ph; 2H, *o*-P^{2}Ph), 7.69–7.60 (2H tot, 1H, *p*-P^{1}Ph; 1H, *p*-P^{2}Ph), 7.47 (td, 2H, $^3J_{HH}$ = 7.9 Hz, $^4J_{HP}$ = 2.8 Hz, *m*-P^{2}Ph), 7.43–7.31 (8H tot; 4H, *m*-P^{1}Ph; 2H, *m*-P^{2}Ph; 1H, *p*-P^{1}Ph; 1H, *p*-P^{2}Ph), 7.27 (m, 2H, *o*-P^{1}Ph), 7.19 (dd, 2H, $^3J_{HP}$ = 11.1 Hz, $^3J_{HH}$ = 7.9 Hz, *o*-P^{2}Ph), 7.03 (dt, 1H, $^3J_{HH}$ = 8.0 Hz, $^4J_{HP}$ = 2.0 Hz, C^{2}H$^{tol\text{-}P1}$), 6.96 (dt, 1H, $^3J_{HH}$ = 8.2 Hz, $^4J_{HP}$ = 1.7 Hz, C^{2}H$^{tol\text{-}P2}$), 6.88 (dd, 1H, $^3J_{HH}$ = 8.0 Hz, $^5J_{HP}$ = 1.0 Hz, C^{3}H$^{tol\text{-}P1}$), 6.74 (dd, 1H, $^3J_{HH}$ = 8.2 Hz, $^5J_{HP}$ = 0.9 Hz, C^{3}H$^{tol\text{-}P2}$), 6.64 (dd, 1H, $^3J_{HH}$ = 8.2 Hz, $^5J_{HP}$ = 1.2 Hz, C^{3}H$^{tol\text{-}P1}$), 6.52 (dd, 1H, $^3J_{HH}$ = 8.2 Hz, $^5J_{HP}$ = 1.4 Hz, C^{3}H$^{tol\text{-}P2}$), 6.09 (dt, 1H, $^3J_{HH}$ = 8.2 Hz, $^4J_{HP}$ = 1.9 Hz, C^{2}H$^{tol\text{-}P1}$), 6.06 (dt, 1H, $^3J_{HH}$ = 8.2 Hz, $^4J_{HP}$ = 1.7 Hz, C^{2}H$^{tol\text{-}P2}$), 5.08 (m, 1H, C^{1}H^{cod}), 4.17 (dd, 1H, $^3J_{HP}$ = 14.1 Hz, $^3J_{HH}$ = 6.0 Hz, C^{2}H^{cod}), 3.89 (m, 1H, C^{3}H^{cod}), 3.67–3.59 (2H tot; 1H, C^{5}H^{cod}; 1H, C^{6}H^{cod}), 3.39 (br, 1H, C^{4}H^{cod}), 3.35–3.19 (2H tot; 1H, C^{4}H^{cod}; 1H, C^{7}H^{cod}), 3.03 (m, 1H, C^{7}H^{cod}), 2.48 (m, 1H, C^{8}H^{cod}), 2.16 (s, 3H, CH$_3^{tol\text{-}P1}$), 2.06 (s, 3H, CH$_3^{tol\text{-}P2}$), 1.69 (m, 1H, C^{8}H^{cod}), 1.28 (s, 3H, CH$_3$Si), −0.35 (s, 3H, CH$_3$Si). ^{13}C NMR (CD_2Cl_2, 298 K): δ_C 138.9 (d, $^2J_{CP}$ = 9.1 Hz, C$^{1,\ tol\text{-}P2}$), 138.3 (d, $^2J_{CP}$ = 8.3 Hz, C$^{1,\ tol\text{-}P1}$), 138.0 (d, $^5J_{CP}$ = 1.5 Hz, C$^{4,\ tol\text{-}P1}$), 137.8 (d, $^5J_{CP}$ = 1.7 Hz, C$^{4,\ tol\text{-}P2}$), 135.2 (br, C$^{2,\ PhP1}$; C$^{2,\ PhP2}$), 134.9 (d, $^2J_{CP}$ = 12.1 Hz, C$^{2,\ PhP2}$), 133.10 (C$^{4,\ PhP1}$), 133.03 (C$^{4,\ PhP2}$), 132.83 (d, $^3J_{CP}$ = 2.4 Hz, C$^{2,\ tol\text{-}P1}$), 132.75 (d, $^2J_{CP}$ = 9.2 Hz, C$^{2,\ PhP2}$), 132.5 (C$^{2,\ tol\text{-}P2}$), 132.4 (d, $^3J_{CP}$ = 3.1 Hz, C$^{2,\ tol\text{-}P2}$), 131.9 (d, $^3J_{CP}$ = 3.0 Hz, C$^{2,\ tol\text{-}P1}$), 130.18 (C$^{3,\ tol\text{-}P1}$), 130.10 (C$^{3,\ tol\text{-}P1}$), 130.03 (C$^{3,\ tol\text{-}P2}$), 129.96 (d, $^3J_{CP}$ = 11.6 Hz, C$^{3,\ PhP2}$), 129.88 (C$^{3,\ tol\text{-}P2}$), 129.4 (d, $^3J_{CP}$ = 11.1 Hz, C$^{3,\ PhP1}$), 128.4 (d, $^3J_{CP}$ = 11.3 Hz, C$^{3,\ PhP2}$), 128.2 (d, $^3J_{CP}$ = 10.3 Hz, C$^{3,\ PhP2}$), 111.7 (d, $^2J_{CP}$ = 14.3 Hz, C$^{6,\ cod}$), 92.2 (C$^{2,\ cod}$), 83.6 (d, $^2J_{CP}$ = 28.1 Hz, C$^{1,\ cod}$), 64.0 (dd, $^2J_{CP}$ = 5.4; 2.9 Hz, C$^{5,\ cod}$), 34.5 (d, $^2J_{CP}$ = 3.4 Hz, C$^{3,\ cod}$), 33.3 (d, $^3J_{CP}$ = 4.5 Hz, C$^{7,\ cod}$), 28.2 (C$^{8,\ cod}$), 21.32 (CH$_3^{tol\text{-}P1}$), 21.23 (CH$_3^{tol\text{-}P2}$), 19.8 (C$^{4,\ cod}$), 5.6 (CH$_3$Si), 5.0 (CH$_3$Si). ^{31}P NMR (CD_2Cl_2, 298 K): δ_P 32.1 (d, $^2J_{PP}$ = 25.3 Hz, P^1), 23.2 (d, $^2J_{PP}$ = 25.3 Hz, P^2).

Synthesis of [Ir$_2${κ^3*C*,*P*,*P*′-(SiNP-H)}$_2$(μ-I)$_3$][PF$_6$] (7aPF$_6$ + 7bPF$_6$). *Method 1.* An acetone solution (5 mL) of [Ir{κ^3*C*,*P*,*P*′-(SiNP-H)}(cod)] (**4**, 98.5 mg, 0.105 mmol, 938.18 g mol^{-1}) was added with ferrocenium hexaphluorophosphate (69.5 mg, 0.210 mmol, 331.00 g mol^{-1}). After 1 h stirring, sodium iodide (23.6 mg, 0.157 mmol, 149.89 g mol^{-1}) was added and the suspension stirred for 1 h. The resulting suspension was filtered, and the solution evaporated up to 2 mL and added with diethyl ether (5 mL), affording a yellow solid which was filtered off, washed with diethyl ether (2 × 5 mL), dried *in vacuo* and finally identified as [Ir$_2${κ^3*C*,*P*,*P*′-(SiNP-H)}$_2$(μ-I)$_3$][PF$_6$] (**7a**PF$_6$ + **7b**PF$_6$) (80.9 mg, 71% yield). *Method 2.* A dichloromethane solution (10 mL) of [Ir{κ^3*C*,*P*,*P*′-(SiNP-H)}(CH$_3$CN)$_3$][PF$_6$]$_2$ (**5**[PF$_6$]$_2$, 119 mg, 95.7 μmol, 1243.09 g mol^{-1}) was added with sodium iodide (21.5 mg, 0.143 mmol, 149.89 g mol^{-1}). The resulting yellow suspension was stirred for 1 h, filtered off, evaporated up to 3 mL and added with diethyl ether (5 mL) affording a yellow solid which was filtered, washed with diethyl ether (3 × 5 mL), dried *in vacuo* and finally identified as [Ir$_2${κ^3*C*,*P*,*P*′-(SiNP-H)}$_2$(μ-I)$_3$][PF$_6$] (**7a**PF$_6$ + **7b**PF$_6$) (90.3 mg, 86% yield). Found: C 43.85, H 3.58, N 2.64. Calcd for $C_{80}H_{78}F_6I_3Ir_2N_4P_5Si_2$ (2185.68 g mol^{-1}): C 43.96, H 3.60, N 2.56. MS (MALDI+, *m*/*z*): calcd for [Ir$_2$(μ-I)$_3${κ^3*C*,*P*,*P*′-(SiNP-H)}$_2$]$^+$ 2041.1; found 2040.8 [M]$^+$. ^{1}H NMR (CD_2Cl_2, 298 K): δ_H 7.42–7.14 (12H tot; 4H, *o*-PPh; 4H, *m*-PPh; 4H, *p*-PPh), 7.05–6.90 (8H tot; 4H, *o*-PPh, 4H, *m*-PPh), 6.70 (d, 4H, $^3J_{HH}$ = 7.3 Hz, *m*-PPh), 7.02–6.90 (m, 4H, *o*-PPh), 6.82 (d, 4H, $^3J_{HH}$ = 8.2 Hz, C^{3}H^{tol}), 6.26 (d, 4H, $^3J_{HH}$ = 8.2 Hz, C^{2}H^{tol}), 2.08 (s, 6H, CH$_3^{tol}$), 2.05 (s, 2H, SiCH$_2$Ir), −0.00 (br, 3H, SiCH$_3$). ^{13}C {^{1}H} NMR (CD_2Cl_2, 298 K): δ_C 140.06 (C$^{1,\ PhP}$), 139.4 (C$^{1,\ PhP}$), 138.8 (C$^{4,\ tol}$), 136.7 (C$^{1,\ tol}$), 136.0 (C$^{2,\ PhP}$), 133.0 (C$^{4,\ PhP}$), 132.5 (d$^3J_{CP}$ = 7.6 Hz, C$^{3,\ PhP}$), 130.5 (C^{3,tol}), 129.6 (C^{2,tol}), 129.0 (C$^{2,\ PhP}$), 128.6 (C$^{3,\ PhP}$), 21.5 (CH$_3^{tol}$), −0.6 (CH$_3$Si), −11.7 (CH$_2$Si). ^{31}P{^{1}H} NMR (CD_2Cl_2, 298 K): δ_P 20.7 (s, SiNP), −144.4 (hept, 1P, $^1J_{PF}$ = 710.3 Hz, PF$_6^-$).

Synthesis of [Ir{κ^3*C*,*P*,*P*′-(SiNP-H)}(η^2,η^3-C$_8$H$_{11}$)][OTf] (8OTf$_3$). A dichloromethane solution (5 mL) of [Ir{κ^3*C*,*P*,*P*′-(SiNP-H)}(cod)] (114 mg, 0.122 mmol, 938.18 g mol^{-1}) was added with methyl trifluoromethylsulphonate (13.9 μL, 0.123 mmol, 164.10 g mol^{-1}, 1.45 g mL^{-1}). After 4 d stirring at room temperature, the solution was evaporated and the residue extracted with acetonitrile/diethyl ether (1 : 20 mL). The solution was dried *in vacuo* affording a colorless solid finally identified as [Ir{κ^3*C*,*P*,*P*′-(SiNP-H)}(η^2,η^3-C$_8$H$_{11}$)][OTf] (**8**OTf) (59.4 mg, 45% yield). Found: C 54.27, H 4.53, N 2.56. Calcd for $C_{49}H_{50}F_3IrN_2O_3P_2SSi$ (1086.24 g mol^{-1}): C 54.18, H 4.64, N 2.58. ^{1}H NMR (CD_2Cl_2, 298 K): δ_H 7.90 (ddd, 2H. $^3J_{HP}$ = 10.4 Hz, $^3J_{HH}$ = 7.6 Hz, $^5J_{HP}$ = 1.2 Hz, *o*-P^{2}Ph), 7.82 (ddd, 2H. $^3J_{HP}$ = 11.2 Hz, $^3J_{HH}$ = 7.6 Hz, $^5J_{HP}$ = 1.9 Hz, *o*-P^{2}Ph), 7.65–7.56 (6H tot; 2H, *o*-P^{1}Ph; 2H, *m*-P^{2}Ph; 2H, *p*-P^{2}Ph), 7.55–7.45 (6H tot; 2H, *m*-P^{1}Ph; 2H, *m*-P^{2}Ph; 2H, *p*-P^{1}Ph), 7.07 (td, 2H, $^3J_{HH}$ = 7.6 Hz, $^4J_{HP}$ = 2.5 Hz, *o*-P^{1}Ph), 7.02 (d, 2H, $^3J_{HH}$ = 8.2 Hz, C^{3}H$^{tol\text{-}P2}$), 6.70 (d, 2H, $^3J_{HH}$ = 8.2 Hz, C^{3}H$^{tol\text{-}P1}$), 6.69 (d, 2H, $^3J_{HH}$ = 8.2 Hz, C^{2}H$^{tol\text{-}P1}$), 6.49 (ddd, 2H, $^3J_{HP}$ = 10.9 Hz, $^3J_{HH}$ = 7.6 Hz, $^5J_{HP}$ = 1.1 Hz, *o*-P^{1}Ph), 6.28 (d, 2H, $^3J_{HH}$ = 8.2 Hz, C^{2}H$^{tol\text{-}P2}$), 4.37–4.32 (2H tot; 1H, C^{2}H^{cod}; 1H, C^{6}H^{cod}), 4.08 (m, 1H, C^{1}H^{cod}), 3.76 (m, 1H, C^{5}H^{cod}), 3.38 (m, 1H, C^{4}H^{cod}), 2.94–2.83 (2H tot; 1H, C^{7}H^{cod}; 1H, C^{4}H^{cod}), 2.52 (m, 1H, C^{7}H^{cod}), 2.30 (s, 3H, CH$_3^{tol\text{-}P2}$), 2.26 (m, 1H, C^{8}H^{cod}), 2.15 (m, 1H, C^{3}H^{cod}), 2.10 (s, 3H, CH$_3^{tol\text{-}P1}$), 1.68 (m, 1H, C^{8}H^{cod}), 0.55 (ddd, 1H, $^2J_{HH}$ = 12.4 Hz, $^3J_{HP}$ = 8.3 Hz, $^3J_{HP}$ = 3.0 Hz, SiCH^{a}H^{b}Ir), 0.46 (ddd, 1H, $^2J_{HH}$ = 12.4 Hz, $^3J_{HP}$ = 7.0 Hz, $^3J_{HP}$ = 2.4 Hz, SiCH^{a}H^{b}Ir), 0.12 (s, 3H, SiCH$_3$). ^{13}C{^{1}H} NMR (CD_2Cl_2, 298 K): δ_C 143.1 (dd, $^1J_{CP}$ = 51.5 Hz, $^3J_{CP}$ = 2.6 Hz, C$^{1,\ PhP1}$), 139.2 (d, $^2J_{CP}$ = 8.0 Hz, C$^{1,\ tol\text{-}P1}$), 138.3 (d, $^2J_{CP}$ = 10.0 Hz, C$^{1,\ tol\text{-}P2}$), 137.4 (d, $^5J_{CP}$ = 1.6 Hz, C$^{4,\ tol\text{-}P2}$), 136.0 (d, $^2J_{CP}$ = 11.9 Hz, C$^{2,\ PhP1}$), 135.5 (C$^{4,\ tol\text{-}P1}$), 133.7 (d, $^2J_{CP}$ = 9.4 Hz, C$^{2,\ PhP2}$), 133.3 (d, $^2J_{CP}$ = 10.7 Hz, C$^{2,\ PhP2}$), 133.1 (d, $^4J_{CP}$ = 2.1 Hz, C$^{4,\ PhP1}$), 132.7 (d, $^4J_{CP}$ = 2.5 Hz, C$^{4,\ PhP2}$), 132.6 (d, $^4J_{CP}$ = 2.4 Hz, C$^{4,\ PhP1}$), 131.8 (d, $^4J_{CP}$ = 1.8 Hz, C$^{4,\ PhP1}$), 130.9 (d, $^4J_{CP}$ = 2.2 Hz, C$^{3,\ tol\text{-}P1}$), 130.7 (d, $^4J_{CP}$ = 1.2 Hz, C$^{3,\ tol\text{-}P2}$), 130.2 (d, $^2J_{CP}$ = 10.2 Hz, C$^{2,\ PhP1}$), 129.9 (C$^{2,\ tol\text{-}P1}$), 129.7 (d, $^3J_{CP}$ = 9.9 Hz, C$^{3,\ PhP1}$), 129.6 (d, $^3J_{CP}$ = 8.7 Hz, C$^{3,\ PhP2}$), 129.4 (d, $^3J_{CP}$ = 10.7 Hz, C$^{3,\ PhP2}$), 128.9 (d, $^3J_{CP}$ = 10.6 Hz, C$^{3,\ PhP1}$), 128.1 (d, $^3J_{CP}$ = 4.1 Hz, C$^{2,\ tol2}$), 106.1 (d, $^2J_{CP}$ = 2.0 Hz, C$^{2\ cod}$), 98.8 (C$^{6\ cod}$), 71.0 (d, $^2J_{CP}$ = 35.7 Hz, C$^{1\ cod}$), 53.9 (d, $^2J_{CP}$ = 3.6 Hz, C$^{5\ cod}$), 49.2 (d, $^2J_{CP}$ = 17.2 Hz, C$^{3\ cod}$), 34.2 (d, $^3J_{CP}$ = 5.3 Hz, C$^{7\ cod}$), 29.4 (d,

$^{3}J_{CP}$ = 3.4 Hz, $C^{8\ cod}$), 21.4 ($CH_3^{tol\text{-}P2}$), 21.0 ($CH_3^{tol\text{-}P1}$), 20.5 (d, $^{3}J_{CP}$ = 4.5 Hz, $C^{4\ cod}$), −1.6 (t, $^{3}J_{CP}$ = 6.9 Hz, CH_3Si), −13.8 (t, $^{2}J_{CP}$ = 4.1 Hz, CH_2Si). $^{31}P\{^{1}H\}$ NMR (CD_2Cl_2, 298 K): δ_P 35.4 (d, 1P, $^{2}J_{PP}$ = 9.1 Hz, SiNP[1]), 31.5 (d, 1P, $^{2}J_{PP}$ = 9.2 Hz, SiNP[2]).

DFT calculations. Molecular structure optimizations and frequencies calculations were carried out with the programs Gaussian09 (revision D.01)[11] or Gaussian16 (revision C.01)[12] using the method B97D3,[13] including the D3 dispersion correction scheme by Grimme with Becke–Johnson damping.[14] The def2-SVP[15] basis and pseudo potential were used for all atoms and the "ultrafine" grid was employed in all calculations. Stationary points were characterized by vibrational analysis. The structures were optimized in dichloromethane (298 K, 1 atm) using the CPCM method.[16]

Crystal structure determination. X-ray diffraction data were collected at 100(2) K on a Bruker SMART APEX (**1**, **6I**) or APEX DUO (**4**, **5**, and **7aPF$_6$**) CCD diffractometers with graphite-monochromated Mo-Kα radiation (λ = 0.71073 Å) using ω rotations. Intensities were integrated and corrected for absorption effects with SAINT-PLUS[17] and SADABS[18] programs, both included in APEX2 package. The structures were solved by the Patterson method with SHELXS-97[19] and refined by full matrix least-squares on F^2 with SHELXL-2014,[20] under WinGX.[21] In the case of 6 and 7 the program SQUEEZE[22] was used to treat the residual electron density.

Crystal data and structure refinement for 1. $C_{45}H_{49}Cl_6IrN_2P_2Si$, 1112.79 g mol^{-1}, monoclinic, $P2_1/c$, a = 9.7848(5) Å, b = 24.1760(13) Å, c = 19.4510(10) Å, β = 91.1030(10)°, V = 4600.4(4) Å^3, Z = 4, D_{calc} = 1.607 g cm^{-3}, μ = 3.381 mm^{-1}, F(000) = 2224, yellow prism, 0.300 × 0.300 × 0.180 mm^3, $\theta_{min}/\theta_{max}$ 1.344/26.373°, index ranges: $-12 \le h \le 12$, $-30 \le k \le 30$, $-24 \le l \le 24$, reflections collected/independent 98 360/9414 [R(int) = 0.0405], T_{max}/T_{min} 0.4045/0.3179, data/restraints/parameters 9414/35/536, GooF(F^2) = 1.035, R_1 = 0.0304 [$I > 2\sigma(I)$], wR_2 = 0.0762 (all data), largest diff. peak/hole 2.050/−1.461 e Å^{-3}. CCDC deposit number 2282657.‡

Crystal data and structure refinement for 4. $C_{99}H_{108}Cl_6Ir_2N_4P_4Si_2$, 2131.05 g mol^{-1}, triclinic, $P\bar{1}$, a = 13.1665(17) Å, b = 13.8662(18) Å, c = 15.261(3) Å, α = 108.940(2)°, β = 90.289(2)°, γ = 118.034(2)°, V = 2284.3(6) Å^3, Z = 1, D_{calc} = 1.549 g cm^{-3}, μ = 3.231 mm^{-1}, F(000) = 1074, colourless prism 0.320 × 0.200 × 0.070 mm^3, $\theta_{min}/\theta_{max}$ 1.437/26.371°, index ranges: $-16 \le h \le 16$, $-16 \le k \le 17$, $-19 \le l \le 18$, reflections collected/independent 20 795/9338 [R(int) = 0.0354], T_{max}/T_{min} 0.5490/0.4262, data/restraints/parameters 9338/1/529, GooF(F^2) = 1.038, R_1 = 0.0326 [$I > 2\sigma(I)$], wR_2 = 0.0847 (all data), largest diff. peak/hole 2.621/−1.325 e Å^{-3}. CCDC deposit number 2282655.‡

Crystal data and structure refinement for 5[CF$_3$SO$_3$]$_2$. $C_{48}H_{48}F_6IrN_5O_6P_2S_2Si$, 1251.26 g mol^{-1}, monoclinic, $P2_1/c$, a = 17.3156(16) Å, b = 21.0500(19) Å, c = 14.0982(13) Å, β = 93.2640(10)°, V = 5130.4(8) Å^3, Z = 4, D_{calc} = 1.620 g cm^{-3}, μ = 2.844 mm^{-1}, F(000) = 2504, colourless prism 0.260 × 0.150 × 0.100 mm^3, $\theta_{min}/\theta_{max}$ 1.178/28.282°, index ranges: $-23 \le h \le 23$, $-26 \le k \le 27$, $-18 \le l \le 18$, reflections collected/independent 52 030/12 697 [R(int) = 0.0512], T_{max}/T_{min} 0.6205/0.4784, data/restraints/parameters 12 697/0/646, GooF(F^2) = 1.014, R_1 = 0.0298 [$I > 2\sigma(I)$], wR_2 = 0.0598 (all data), largest diff. peak/hole 1.039/−0.685 e Å^{-3}. CCDC deposit number 2282656.‡

Crystal data and structure refinement for 6I. $C_{51}H_{57}Cl_6I_2IrN_2P_2Si$, 723.36 g mol^{-1}, triclinic, $P\bar{1}$, a = 10.3680(8) Å, b = 14.1270(11) Å, c = 19.6166(16) Å, α = 100.9810(10)°, β = 98.2830(10)°, γ = 103.0900(10)°, V = 2694.2(4) Å^3, Z = 2, D_{calc} = 1.783 g cm^{-3}, μ = 4.040 mm^{-1}, F(000) = 1412, orange prism, 0.250 × 0.140 × 0.090 mm^3, $\theta_{min}/\theta_{max}$ 2.056/26.372°, index ranges $-12 \le h \le 12$, $-17 \le k \le 17$, $-24 \le l \le 24$, reflections collected/independent 39 544/10 963 [R(int) = 0.0353], T_{max}/T_{min} 0.5264/0.3558, data/restraints/parameters 10 963/0/540, GooF(F^2) = 1.052, R_1 = 0.0372 [$I > 2\sigma(I)$], wR_2 = 0.0949 (all data), largest diff. peak/hole 2.043/−1.903 e Å^{-3}. CCDC deposit number 2282659.‡

Crystal data and structure refinement for 7aPF$_6$. $C_{87}H_{94}Cl_2F_6I_3Ir_2N_4P_5Si_2$, 2356.69 g mol^{-1}, monoclinic, $P2_1/n$, a = 21.602(9) Å, b = 18.519(8) Å, c = 22.985(10) Å, β = 104.342(8)°, V = 8908(7) Å^3, Z = 4, D_{calc} = 1.757 g cm^{-3}, μ = 4.260 mm^{-1}, F(000) = 4592, yellow prism 0.300 × 0.230 × 0.180 mm^3, $\theta_{min}/\theta_{max}$ 1.158/25.027°, index ranges $-25 \le h \le 25$, $-21 \le k \le 22$, $-25 \le l \le 27$, reflections collected/independent 60 741/15 721 [R(int) = 0.0406], T_{max}/T_{min} 0.3444/0.2500, data/restraints/parameters 15 721/4/913, GooF(F^2) = 1.016, R_1 = 0.0303 [$I > 2\sigma(I)$], wR_2 = 0.0753 (all data), largest diff. peak/hole 2.080/−1.144 e Å^{-3}. CCDC deposit number 2282658.‡

Conflicts of interest

There are no conflicts to declare.

Acknowledgements

Financial support from the Spanish Ministerio de Ciencia e Innovación MCIN/AEI/10.13039/501100011033, under the project PID2019-103965GB-I00, and the Departamento de Ciencia, Universidad y Sociedad del Conocimiento del Gobierno de Aragón (group E42_23R) is gratefully acknowledged.

References

1 (*a*) G. Ewart, D. S. Payne, A. L. Porte and A. P. Lane, *J. Chem. Soc.*, 1962, 3984; (*b*) H. H. Sisler and N. L. Smith, *J. Org. Chem.*, 1961, **26**, 611; (*c*) W. A. Hart and H. H. Sisler, *Inorg. Chem.*, 1964, **3**, 617–622.

2 Selected references: (*a*) K. M. Gramigna, D. A. Dickie, B. M. Foxman and C. M. Thomas, *ACS Catal.*, 2019, **9**, 3153–3164; (*b*) A. M. Lifschitz, N. A. Hirscher, H. B. Lee, J. A. Buss and T. Agapie, *Organometallics*, 2017, **36**, 1640–1648; (*c*) A. Prades, S. Núñez-Pertíñez, A. Riera and X. Verdaguer, *Chem. Commun.*, 2017, **53**, 4605–4608; (*d*) S. A. Bartlett, J. Moulin, M. Tromp, G. Reid, A. J. Dent, G. Cibin, D. S. McGuinness and J. Evans, *Catal. Sci.*

Technol., 2016, **6**, 6237–6246; (*e*) S. Orgué, T. León, A. Riera and X. Verdaguer, *Org. Lett.*, 2015, **17**, 250–253; (*f*) W. K. Walker, B. M. Kay, S. A. Michaelis, D. L. Anderson, S. J. Smith, D. H. Ess and D. J. Michaelis, *J. Am. Chem. Soc.*, 2015, **137**, 7371–7378; (*g*) W. K. Walker, D. L. Anderson, R. W. Stokes, S. J. Smith and D. J. Michaelis, *Org. Lett.*, 2015, **17**, 752–755; (*h*) F. Trentin, A. M. Chapman, A. Scarso, P. Sgarbossa, R. A. Michelin, G. Strukul and D. F. Wass, *Adv. Synth. Catal.*, 2012, **354**, 1095–1104; (*i*) L. E. Bowen, M. Charernsuk, T. W. Hey, C. L. McMullin, A. G. Orpen and D. F. Wass, *Dalton Trans.*, 2010, **39**, 560–567; (*j*) B. R. Aluri, N. Peulecke, B. H. Müller, S. Peitz, A. Spannenberg, M. Hapke and U. Rosenthal, *Organometallics*, 2010, **29**, 226–231.

3 Selected references: (*a*) A. Aloisi, É. Crochet, E. Nicolas, J.-C. Berthet, C. Lescot, P. Thuéry and T. Cantat, *Organometallics*, 2021, **40**, 2064–2069; (*b*) H. Zhang, G. P. Hatzis, C. E. Moore, D. A. Dickie, M. W. Bezpalko, B. M. Foxman and C. M. Thomas, *J. Am. Chem. Soc.*, 2019, **141**, 9516–9520; (*c*) H. Zhang, B. Wu, S. L. Marquard, E. D. Litle, D. A. Dickie, M. W. Bezpalko, B. M. Foxman and C. M. Thomas, *Organometallics*, 2017, **36**, 3498–3507; (*d*) J. P. Krogman, B. M. Foxman and C. M. Thomas, *Organometallics*, 2015, **34**, 3159–3166.

4 Selected references: (*a*) C. Mu, J. He, S. Lü, J. Yang, Y. Xie, K. Hu, P. Yan and Y.-L. Li, *Polyhedron*, 2021, **200**, 115087; (*b*) L.-C. Song, L.-D. Zhang, W.-W. Zhang and B.-B. Liu, *Organometallics*, 2018, **37**, 1948–1957; (*c*) L.-C. Song, X.-F. Han, W. Chen, J.-P. Li and X.-Y. Wang, *Dalton Trans.*, 2017, **46**, 10003–10013.

5 Selected references: (*a*) B. S. Mitchell, W. Kaminsky and A. Velian, *Inorg. Chem.*, 2021, **60**, 6135–6139; (*b*) J. A. Kephart, A. C. Boggiano, W. Kaminsky and A. Velian, *Dalton Trans.*, 2020, **49**, 16464–16473; (*c*) B. A. Barden, G. Culcu, J. P. Krogman, M. W. Bezpalko, G. P. Hatzis, D. A. Dickie, B. M. Foxman and C. M. Thomas, *Inorg. Chem.*, 2019, **58**, 821–833; (*d*) G. Culcu, D. A. Iovan, J. P. Krogman, M. J. T. Wilding, M. W. Bezpalko, B. M. Foxman and C. M. Thomas, *J. Am. Chem. Soc.*, 2017, **139**, 9627–9636; (*e*) S. Todisco, V. Gallo, P. Mastrorilli, M. Latronico, N. Re, F. Creati and P. Braunstein, *Inorg. Chem.*, 2012, **51**, 11549–11561.

6 V. Passarelli and F. Benetollo, *Inorg. Chem.*, 2011, **50**, 9958–9967.

7 (*a*) V. Passarelli, J. J. Pérez-Torrente and L. A. Oro, *Inorg. Chem.*, 2014, **53**, 972–980; (*b*) V. Passarelli, J. J. Pérez-Torrente and L. A. Oro, *Dalton Trans.*, 2015, **44**, 18596–18606; (*c*) V. Passarelli, J. J. Pérez-Torrente and L. A. Oro, *Dalton Trans.*, 2016, **45**, 951–962; (*d*) M. Palmese, J. J. Pérez-Torrente and V. Passarelli, *Dalton Trans.*, 2022, **51**, 7142–7153; (*e*) M. Palmese, J. J. Pérez-Torrente and V. Passarelli, *Dalton Trans.*, 2022, **51**, 12334–12351.

8 Selected references: (*a*) S. W. Kim, C. C. Meyer, B. K. Mai, P. Liu and M. J. Krische, *ACS Catal.*, 2019, **9**, 9158–9163; (*b*) D. C. Schmitt, A.-M. R. Dechert-Schmitt and M. J. Krische, *Org. Lett.*, 2012, **14**, 6302–6305; (*c*) I. S. Kim, M.-Y. Ngai and M. J. Krische, *J. Am. Chem. Soc.*, 2008, **130**, 14891–14899.

9 K. M. Altus and J. A. Love, *Commun. Chem.*, 2021, **4**, 173.

10 (*a*) C. Tejel, M. A. Ciriano, V. Passarelli, J. A. López and B. De Bruin, *Chem. – Eur. J.*, 2008, **14**, 10985–10998; (*b*) M. Martin, W. Sola, O. Torres, P. Plou and L. A. Oro, *Organometallics*, 2003, **22**, 5406–5417; (*c*) R. Dorta and A. Togni, *Organometallics*, 1998, **17**, 5441–5444; (*d*) G. W. Bushnell, D. O. Kim Fjeldsted, S. R. Stobart and M. J. Zaworotko, *J. Chem. Soc., Chem. Commun.*, 1983, 580–581; (*e*) D. R. Russell and P. A. Tucker, *J. Organomet. Chem.*, 1977, **125**, 303–312.

11 M. J. Frisch, G. W. Trucks, H. B. Schlegel, G. E. Scuseria, M. A. Robb, J. R. Cheeseman, G. Scalmani, V. Barone, B. Mennucci, G. A. Petersson, H. Nakatsuji, M. Caricato, X. Li, H. P. Hratchian, A. F. Izmaylov, J. Bloino, G. Zheng, J. L. Sonnenberg, M. Hada, M. Ehara, K. Toyota, R. Fukuda, J. Hasegawa, M. Ishida, T. Nakajima, Y. Honda, O. Kitao, H. Nakai, T. Vreven, J. A. Montgomery Jr., J. E. Peralta, F. Ogliaro, M. Bearpark, J. J. Heyd, E. Brothers, K. N. Kudin, V. N. Staroverov, R. Kobayashi, J. Normand, K. Raghavachari, A. Rendell, J. C. Burant, S. S. Iyengar, J. Tomasi, M. Cossi, N. Rega, J. M. Millam, M. Klene, J. E. Knox, J. B. Cross, V. Bakken, C. Adamo, J. Jaramillo, R. Gomperts, R. E. Stratmann, O. Yazyev, A. J. Austin, R. Cammi, C. Pomelli, J. W. Ochterski, R. L. Martin, K. Morokuma, V. G. Zakrzewski, G. A. Voth, P. Salvador, J. J. Dannenberg, S. Dapprich, A. D. Daniels, C. Farkas, J. B. Foresman, J. V. Ortiz, J. Cioslowski and D. J. Fox, *Gaussian 09, Revision D.01*, Gaussian, Inc., Wallingford CT, 2009.

12 M. J. Frisch, G. W. Trucks, H. B. Schlegel, G. E. Scuseria, M. A. Robb, J. R. Cheeseman, G. Scalmani, V. Barone, G. A. Petersson, H. Nakatsuji, X. Li, M. Caricato, A. V. Marenich, J. Bloino, B. G. Janesko, R. Gomperts, B. Mennucci, H. P. Hratchian, J. V. Ortiz, A. F. Izmaylov, J. L. Sonnenberg, D. Williams-Young, F. Ding, F. Lipparini, F. Egidi, J. Goings, B. Peng, A. Petrone, T. Henderson, D. Ranasinghe, V. G. Zakrzewski, J. Gao, N. Rega, G. Zheng, W. Liang, M. Hada, M. Ehara, K. Toyota, R. Fukuda, J. Hasegawa, M. Ishida, T. Nakajima, Y. Honda, O. Kitao, H. Nakai, T. Vreven, K. Throssell, J. A. Montgomery Jr., J. E. Peralta, F. Ogliaro, M. J. Bearpark, J. J. Heyd, E. N. Brothers, K. N. Kudin, V. N. Staroverov, T. A. Keith, R. Kobayashi, J. Normand, K. Raghavachari, A. P. Rendell, J. C. Burant, S. S. Iyengar, J. Tomasi, M. Cossi, J. M. Millam, M. Klene, C. Adamo, R. Cammi, J. W. Ochterski, R. L. Martin, K. Morokuma, O. Farkas, J. B. Foresman and D. J. Fox, *Gaussian 16, Revision C.01*, Gaussian, Inc., Wallingford CT, 2019.

13 A. D. Becke, *J. Chem. Phys.*, 1997, **107**, 8554–8560.

14 S. Grimme, S. Ehrlich and L. Goerigk, *J. Comput. Chem.*, 2011, **32**, 1456–1465.

15 F. Weigend and R. Ahlrichs, *Phys. Chem. Chem. Phys.*, 2005, **7**, 3297–3305.

16 J. Tomasi, B. Mennucci and R. Cammi, *Chem. Rev.*, 2005, **105**, 2999–3093.
17 *SAINT+: Area-Detector Integration Software, version 6.01*, Bruker AXS, Madison, WI, 2001.
18 G. M. Sheldrick, *SADABS program*, University of Göttingen, Göttingen, Germany, 1999.
19 G. M. Sheldrick, *SHELXS 97, Program for the Solution of Crystal Structure*, University of Göttingen, Göttingen, Germany, 1997.
20 G. M. Sheldrick, *Acta Crystallogr., Sect. C: Struct. Chem.*, 2015, **71**, 3–8.
21 L. J. Farrugia, *J. Appl. Crystallogr.*, 2012, **45**, 849–854.
22 A. L. Spek, *Acta Crystallogr., Sect. C: Struct. Chem.*, 2015, **71**, 9–18.